Plant Soil
https://doi.org/10.1007/s11104-024-06655-1

RESEARCH ARTICLE

Soil phosphorus availability affects niche characteristics of dominant C_3 perennial and sub-dominant C_4 annual species in a typical temperate grassland of northern China

Weiyuan Zhang · Jirui Gong · Siqi Zhang · Hans Lambers · Xuede Dong · Yuxia Hu · Guisen Yang · Chenyi Yan

Received: 26 August 2023 / Accepted: 28 March 2024

Abstract

Aims Phosphorus (P) addition can help restore degraded Chinese grasslands. Soil P-availability affects the plant niche dynamics. However, the dynamics of niche characteristics are not yet understood, particularly for above- and belowground differences between species and plant–microbe interactions that generate these dynamics.

Methods We conducted a long-term field P-fertilization experiment (0 to 12.5 g P m^{-2} $year^{-1}$) to explore the impacts of P addition on the niche dynamics of a competitive forb (*Chenopodium aristatum*, a non-mycorrhizal C_4 plant) and a dominant grass (*Leymus chinensis*, a mycorrhizal C_3 plant) in a temperate grassland in Inner Mongolia, northern China.

Results Phosphorus addition greatly changed the niche and exacerbated aboveground competition between *C. aristatum* and *L. chinensis*. Competitive exclusion of *L. chinensis* occurred at all levels, except $P_{2.5}$. Photosynthesis and above- and belowground morphology of *C. aristatum* responded more to P_1 due to its high photosynthetic plasticity and nutrient resorption, which was associated with its competitive advantage. Although *NO* peaked at $P_{2.5}$, carbon assimilation and rhizosheath microbial biomass of *L. chinensis* were optimal. Alleviated *NO* at P_5 and $P_{12.5}$ was associated with segregation of root morphologies and rhizosheath microbial composition. However, surplus niches at P_5 and $P_{12.5}$ were occupied by invasive sub-shrubs, associating with the mismatched plant–microbe feedbacks of *C. aristatum* and *L. chinensis*.

Conclusions Our findings suggest that rhizosheath microbes mediate trade-offs between a host plant's P-conservation and acquisition and highlight the importance of above- and belowground co-responses to community productivity and stability under P addition.

Responsible Editor: Adamo Domenico Rombolà.

Supplementary Information The online version contains supplementary material available at https://doi.org/10.1007/s11104-024-06655-1.

W. Zhang · J. Gong · S. Zhang · X. Dong · Y. Hu · G. Yang · C. Yan
State Key Laboratory of Earth Surface Processes and Resource Ecology, MOE Engineering Research Center of Desertification and Blown-sand Control, Faculty of Geographical Science, Beijing Normal University, Beijing 100875, China

J. Gong (✉)
State Key Laboratory of Earth Surface Processes and Resource Ecology, School of Natural Resources, Faculty of Geographical Science, Beijing Normal University, Beijing 100875, China
e-mail: jrgong@bnu.edu.cn

H. Lambers
School of Biological Sciences, Institute of Agriculture, University of Western Australia, Crawley, Perth, WA 6009, Australia

Published online: 08 April 2024

Keywords Phosphorus fertilization · Niche characteristics · Microbes · Photosynthesis · GAM

Introduction

Grassland ecosystems play an important role in maintaining biodiversity, the global carbon balance, and soil stability in terrestrial ecosystems (Shi et al. 2021). In China, grasslands account for 41.7% of the total land area, and provide 3×10^8 to 4×10^8t of high-quality forage every year (Xu et al. 2013). However, most grassland ecosystems are facing degradation, threatening their forage yield and ability to provide ecosystem services (Graux et al. 2020). Phosphorus (P) is a limiting factor for productivity in many grasslands (Gong et al. 2020). Severe P deficiencies in grasslands result from unsustainable grazing, global climate change, and long-term nitrogen (N) deposition (Bai et al. 2008; Díaz et al. 2006; Lie et al. 2022). Reasonable P-fertilization levels alleviate P deficiency in grassland ecosystems and maintain productivity (Cordell et al. 2009). Nonetheless, P-addition increases above-ground biomass but may also alters the niche characteristics of species, thereby reducing species richness (van der Sande et al. 2017). Hence, determining how species spatial assembling and grassland productivity and stability respond to a soil P availability gradient can support efforts to improve the knowledge of the ecological niche theory and improve management of P fertilization under global change (Reich et al. 2003; Higgins et al. 2012; Freschet et al. 2020; Qaswar et al. 2020).

Long-term P fertilization strongly influences an ecosystem's functional composition, which greatly influences grassland productivity and stability (García-Palacios et al. 2018; Li et al. 2021). In general, the relative dominance of grasses, specifically the herbaceous plants in Gramineae family, strongly contributes to the stability of grassland in northern China (Chen et al. 2016). Soil P availability critically affects the niche dynamics of coexisting plant (Wassen et al. 2021). Unfortunately, inappropriate P addition may promote the relative dominance of competing forbs and shrubs, causing a decrease in grassland stability (Liu et al. 2018). The competition–facilitation and displacement–coexistence processes under P-addition gradient between coexisting grasses, forbs and shrubs lead to niche overlap (*NO*) and differentiation (Ashton et al. 2010; Holt 2009; Silvertown 2004; Ávila-Lovera et al. 2021). Under high P-addition, species with large niche width, typically forbs, could effectively utilized the increased P availability, gaining a competitive advantage in inter-species competition and leading to lower species diversity (Austin and Meyers 1996; Richardson et al. 2011). Conversely, under proper edaphic P level, species richness can be drove by niche differentiation resulting from diverse P strategies (Phoenix et al. 2020). Therefore, it is necessary to improve our understanding of the responses of niche characteristics of a grassland's dominant grass and forb species to P addition and the underlying mechanisms that determine these responses.

Responses of niche characteristics to P addition result from changes of P acquisition and internal P utilization of different species, which is presenting by above- and belowground morphological and physiological changes (Lejeune et al. 2006; Ávila-Lovera et al. 2021). Phosphorus addition may increase the species richness and aboveground biomass of a grassland community, leading to more intense interspecific competition (Liu et al. 2018). Different responses of vegetation cover and plant height of different functional groups to P fertilization could result in stronger competition for light resources (Copeland et al. 2019; Happonen et al. 2022). In turn, changes in light resources directly affect the photosynthetic activity of plants (Wang et al. 2020). Fast-growing C_4 forbs with higher photosynthetic P-use efficiency probably decrease the photosynthesis of co-existing C_3 grasses by competition for light, resulting in competitive exclusion under P addition (Ghannoum et al. 2008; Harpole and Suding 2011). Moreover, the photosynthetic advantages of C_4 plants may be increased under P addition due to their higher light harvesting capacity of PSII compared with that of C_3plants (Su et al. 2021; Sun et al. 2021). In addition, soil P availability strongly affects plant P status, thereby reducing nutrient-resorption efficiency (Hayes et al. 2014). Species with high N-resorption efficiency under high P addition can maintain a high chlorophyll concentration, and this increases their competitiveness in plant communities (Fiorentini et al. 2019; Yang 2018). Hence, it is critical to explore the responses of the morphology, photosynthesis, chlorophyll fluorescence, and nutrient resorption of coexisting

species with different photosynthetic pathways to P-addition levels through field investigations.

Belowground morphological and physiological changes under P fertilization alter P acquisition of different species, thereby changing their niche characteristics, and higher functional diversity promotes niche differentiation, which mitigates the negative effects of niche overlap on community stability (Jacoby and Kopriva 2019; Kramer-Walter et al. 2016). Segregation of root architecture occurs under different soil P availabilities (Walk et al. 2006). More shallow roots, which are more conducive to absorption of P from the upper soil, are found in P-deficient soil; in contrast, deeper roots are found in fertile soil (Lynch and Brown 2008; Garlick et al. 2021; Wen et al. 2021). The root morphological variability of perennials and annuals under P addition affects species coexistence (Aschehoug and Callaway 2014). Annual forbs usually have finer roots, which favor P absorption and are effective in a soil with a high P availability, whereas perennial grasses usually have coarser roots, which tend to be more heavily colonized by arbuscular mycorrhizal fungi (AMF) and are effective in a soil with a moderately low P availability; P addition can modify these root morphological patterns (Burns et al. 2013; Ma et al. 2018; Wen et al. 2019). Moreover, a higher soil phosphatase activity from microbes promotes niche separation because it potentially widens the range of P resources available to the roots (Turner et al. 2018). Organic P mineralization by microbes is affected by both P supply and C source (Shi et al. 2023). Most herbaceous plant release C into the rhizosphere as root exudates, thus maintaining a functional microbial community, in which phosphatase activity may be altered differently from that in annual species under P addition (Kidd et al. 2018; Moran 2017; Spohn et al. 2013; Sullivan et al. 2014). Hence, unraveling how root morphology and the rhizosphere microbial community respond to P addition will improve our understanding of the mechanisms driving niche segregation.

Patterns of plant–microbe feedbacks link above- and belowground responses under P addition (Hata et al. 2018; Moran 2017). Plant P status is determined by the plant's internal P-resorption efficiency (*PRE*) and external soil P acquisition (Cleveland et al. 2013). Patterns of N: P resorption ratios (*NRE*/*PRE*) have the potential to reflect gradients in plant P limitation (Cleveland et al. 2013; Du et al. 2020; Reed et al. 2012). For external soil P acquisition, acid phosphatase per unit of microbial biomass carbon in the rhizosphere imply increased acid phosphatase release by root exudation (Peng et al. 2023; Raiesi and Beheshti 2014). Along a P-availability gradient, there are trade-offs between internal P resorption and external soil P acquisition which greatly affect a plant's niche (Peng et al. 2023; Wassen et al. 2021). These trade-offs are influenced by the rhizosheath microbial N/P stoichiometry, which is mainly affected by soil P availability (Zhang et al. 2016). High P addition may intensify N deficiency in microbes more than in plants, leading to a difference in the limiting nutrient for plants and microbes and to an N/P stoichiometric imbalance (DeForest 2019; DeForest et al. 2021). These imbalances may change relationships between microbes and their host plants from symbiotic to parasitic (Pathak and Nallapeta 2014; Su et al. 2021). As N resorption of host plants may not compensate for the negative effects of rhizosheath microbes, the competitiveness of the host plants may decrease. Thus, an experiment with multiple levels of P addition would reveal the N/P stoichiometric thresholds that limit plants and microbes, and understanding these thresholds is crucial for finding suitable P addition levels to broaden the niche of desirable dominant species.

To fill some of the gaps in our knowledge, we conducted a long-term P-addition field experiment to explore the impacts of P-addition levels on an ecosystem's functional group composition, niche characteristics, plant morphology, photosynthesis, chlorophyll fluorescence, nutrient resorption, rhizosheath microbial compositions, soil phosphatase activities, and C: N: P stoichiometry of plant–microbe feedbacks for *C. aristatum* (a non-mycorrhizal C_4 forb) and *L. chinensis* (a perennial rhizomatous mycorrhizal C_3 grass) in a typical temperate grassland of northern China. We tested three hypotheses: (1) *C. aristatum* will increasingly occupy the niche of *L. chinensis* under increasing P addition, associated with its more responsive photosynthetic characteristics; (2) P addition will modify root morphology, architecture, and rhizosheath microbial community composition of *L. chinensis* and *C. aristatum*, thereby promoting the niche separation of these two species, and (3) medium P addition will promote both carbon assimilation and rhizosheath microbial biomass of *L. chinensis*, whereas high P addition leads to an imbalanced N/P stoichiometry between plants and microbes.

Materials and methods

Study site

Our study was conducted in a grassland ecosystem in Inner Mongolia, China (44°48'N to 44°49'N, 116°02'E to 116°30'E) with a temperate semi-arid continental climate. The mean monthly temperatures ranges from −21 °C in January to 19 °C in August, and annual precipitation averages 300 mm (Luo et al. 2017). Nearly 80% of precipitation falls during the growing season from May to September (Luo et al. 2017). In August 2018, the average temperature was 19℃ and the total precipitation in that month was 88 mm. The soil type was classified as a Calcic-orthic Aridisol (based on USDA Soil Taxonomy) and Haplic Calcisols (based on FAO). The soil is composed of 60% sand, 21% clay, and 19% silt, with its formation originating from eolian parent material. The dominant species is the mycorrhizal C_3 grass *Leymus chinensis* (Shi et al. 2021).

Experimental design

The experimental site has been fenced since 2009. Soil properties before fertilization were presented in Table 1. Soil (0 to 40 cm) pH was determined by a glass electrode, total carbon and nitrogen concentration (soil [C] and [N]) were determined by CN802, total potassium, calcium, aluminum and sodium concentration (soil [K], [Ca], [Al], and [Na]) were determined by ICP-OES, and plant-available soil phosphorus concentration (Olsen [P]) was determined by a spectrophotometer, these methods of determinations were described below. The plant-available soil P concentration (Olsen [P]) was 2.5 mg kg^{-1} at that time, which is lower than the average concentration of 5.5 mg kg^{-1} in Inner Mongolia (http://www.imaaahs.ac.cn/). Based on this P concentration, we designed five P-addition treatments (control, P_1, $P_{2.5}$, P_5, and $P_{12.5}$) with P fertilizer (orthophosphate, NaH_2PO_4) used to create a gradient of soil P with additions of 0, 1, 2.5, 5, and 12.5 g P m^{-2} $year^{-1}$, respectively. At the designated site, we implemented a randomized block design, consisting of three blocks serving as replicates, separated by a 1.5-meter buffer. Within each block, we arbitrarily set up plots measuring 6 m x 6 m (resulting in 15 plots, derived from 5 P treatments and 3 replicates). Phosphorus fertilization has been carried out once per year at the beginning of each growing season since 2014.

Table 1 Soil (0 to 40 cm) pH, total carbon concentration (soil [C]), total nitrogen concentration (soil [N]), total potassium concentration (soil [K]), total calcium concentration (soil [Ca]), total aluminum concentration (soil [Al]), total sodium concentration (soil [Na]), and plant-available soil phosphorus concentration (Olsen [P]) before fertilization in 2014

Traits	Value
pH	7.71 (0.09)
Soil [C] (g kg^{-1})	20.77 (1.10)
Soil [N] (g kg^{-1})	1.57 (0.07)
Soil [K] (g kg^{-1})	19.36 (0.54)
Soil [Ca] (g kg^{-1})	38.04 (4.02)
Soil [Al] (g kg^{-1})	40.81 (2.79)
Soil [Na] (g kg^{-1})	15.50 (0.27)
Olsen [P] (mg kg^{-1})	2.47 (0.45)

The values are means (SE) ($n = 3$)

Classification of functional groups, niche characteristics and overlap, and aboveground growth rate

Sampling and investigation of the plant community was carried out at the peak of the growing season (August) in 2018, around the time of peak biomass (Bai et al. 2010). We randomly selected three quadrats (0.5 m × 0.5 m) in each plot, identified each plant species, and determined the average height, vegetation cover (% of soil surface), density (number per m^2), and frequency of each species in each plot. Species were classified into five functional groups: perennial rhizomatous grasses (*PRs*: *Leymus chinensis*), perennial bunchgrasses (*PBs*: *Cleistogenes squarrosa* and *Stipa grandis*), perennial forbs (*PFs*: *Thalictrum petaloideum*, *Carex breviculmis*, *Melilotoides ruthenicus*, *Convolvulus ammannii*, and *Medicago sativa*), annuals (*ANs*: *Chenopodium aristatum*, *Salsola collina*, and *Chenopodium glaucum*), and subshrubs (*SSs*: *Artemisia frigida*). Based on these data, we calculated the number of species (*S*) and the relative cover (*RC*), relative density (*RD*), relative height (*RH*), and relative frequency (*RF*) of each species, then calculated the importance value (*IV*; Simpson 1949) of each species, the Simpson index, the Shannon–Wiener index, and Pielou's index of the communities, as well as the niche overlap (*NO*; Pianka 1973)

of *C. aristatum* and *L. chinensis* in the five P-addition treatments (units for all variables used in the equations were presented in Table S1):

$$IV_{ij} = \frac{RC_{ij} + RD_{ij} + RH_{ij} + RF_{ij}}{4} \quad (1)$$

$$\text{Simpson index} = 1 - \sum_{i=1}^{S} IV_{ij}^2 \quad (2)$$

$$\text{Shannon-Wiener index} = -\sum_{i=1}^{S} IV_{ij} lnIV_{ij} \quad (3)$$

$$\text{Pielou's } E = H'/\ln S \quad (4)$$

$$\text{Pianka's } NO = \frac{\sum_{j=1}^{r} \left(IV_{ij} \times IV_{kj}\right)}{\sqrt[2]{\sum_{j=1}^{r} IV_{ij}^2 \times \sum_{j=1}^{r} IV_{kj}^2}} \quad (5)$$

Where IV_{ij} is the importance value of species i in quadrat j; IV_{kj} is the importance value of species k in quadrat j; N_i is the total importance value of species i; r is the number of quadrats; and the range of NO is [0, 1].

We also calculated the niche optima and the borders of niche width of each species on the soil available P gradient using mathematical models. Integrating the method by Boisson et al. (2020), we opted for the Generalized Additive Model (GAM) with a restricted maximum likelihood (REML) to simulate the relative density of each species along the P-addition gradient. The best-fitting model was selected based on the Akaike Information Criterion (AIC) from three levels of smoothness (3, 4, or 5), choosing the model with the lowest AIC value. The modeling and extraction of response curve values were conducted using the 'mgcv' and 'gratia' packages in *R* statistical software.

We harvested the plants in each quadrat at the same time. Aboveground parts of the same species in each quadrat were placed in the same bag. The samples were taken back to the laboratory, placed in an oven, and dried at 65℃ to a constant weight, and then weighed to determine the mean aboveground biomass (*AGB*) of each species and functional group in each plot.

We also collected three to five representative intact individuals of *C. aristatum* and *L. chinensis* with uniform size in each plot in early July and August of 2018 and measured their individual aboveground biomass. We calculated the aboveground growth rate (*AGR*) as follows:

$$AGR = \frac{AGB_{\text{August}} - AGB_{\text{July}}}{\text{time}} \quad (6)$$

Sampling, photosynthetic and fluorescence measurements, and morphological similarity

Sampling and investigation of photosynthesis, fluorescence and morphology were carried out on 15th August in 2018. In each plot, we chose 10 to 15 undamaged individuals of *C. aristatum* and *L. chinensis* with uniform size and used their mature leaves to measure the net photosynthetic rate (A) and stomatal conductance (g_s). We measured the photosynthetic light response (over a range of light intensities from 0 to 2500 μmol m^{-2} s^{-1} photosynthetic photon flux density [PPFD]) and measured CO_2-response curves (under 1500 μmol m^{-2} s^{-1} PPFD and a CO_2 concentration gradient from 0 to 1800 μmol mol^{-1}) between 09:00 and 11:00 using a portable photosynthesis system (LI-6400XT; LI-COR, Lincoln, NE, USA). We calculated the intrinsic water-use efficiency (*iWUE*) as A/g_s (Guerrieri et al. 2019). We computed the maximum photosynthetic rate (A_{max}) and light-saturation point (*LSP*) using the method of (Ye 2007), and the maximum carboxylation efficiency (V_{cmax}) and maximum electron transport rate (J_{max}) based on the methods of Farquhar et al. (1980).

We measured chlorophyll fluorescence with a fluorescence meter (LI-6400XT-40a; LI-COR, Lincoln, NE, USA). Before measuring each sample, leaves were wrapped with tinfoil for more than 40 min to allow dark adjustment. We then recorded the maximum fluorescence (F_m) and minimum fluorescence (F_o) in the dark. Next, we allowed the same leaves to undergo light adjustment at 200 μmol m^{-2} s^{-1} PPFD for 20 min, and then measured the minimum fluorescence in the light (F_o'), maximum fluorescence in the light (F_m'), variable fluorescence (F_v), and the steady-state fluorescence (F_s) after A stabilized. After these measurements, we calculated the maximum quantum efficiency of photosystem II (PSII; F_v/F_m) and quantum efficiency of PSII (F_v'/F_m') (Demmig-Adams et al. 1996; Maxwell and Johnson 2000) as follows:

$$F_v/F_m = \left(F_m - F_o\right)/F_m \quad (7)$$

$$F_{v'}/F_{m'} = \left(F_{m'} - F_{o'}\right)/F_{m'} \quad (8)$$

We then excavated the plants used for the gas-exchange measurements in each plot, aiming to avoid damaging the roots as much as possible, and marked the roots at a depth of 5 cm below the surface to identify the near-surface roots. Roots of other species were removed. These individuals were used to determine the leaf area (*LA*), specific leaf area (*SLA*, which equals *LA* divided by the oven-dry leaf weight), root biomass, fine root morphology, and the manganese (Mn) and total chlorophyll (*TC*) concentrations of the mature leaves and the C, N, and P concentrations of the mature leaves and fresh leaf litter. We calculated the similarity of height and leaf area as:

$$\text{Plant height similarity} = 1 - \left(height_{ij} - height_{kj}\right)/height_{ij} \quad (9)$$

$$LA \text{ similarity} = 1 - \left(LA_{ij} - LA_{kj}\right)/LA_{ij} \quad (10)$$

where $height_{ij}$ and LA_{ij} are the mean plant height and mean *LA* of species *i* in quadrat *j*, respectively, and $height_{kj}$ or LA_{kj} is the mean plant height and mean *LA* of species *k* in quadrat *j*, respectively.

We extracted chlorophyll from the mature leaves using 95% (v/v) ethanol in darkness at 25 °C. We then measured and calculated the total chlorophyll concentration (*TC*) using the equations of Fargašová (1996). We then calculated the total chlorophyll concentration per unit leaf area (Chl_{Total}) as $TC \times SLA$.

We defined the rhizosheath soil as the soil that adhered to the roots after shaking the plants to remove loose soil (Li et al. 2007), pH, acid phosphatase (AP) activity, soil microbial biomass P, C, and N, and microbial phospholipid fatty acids (PLFAs; as detailed below).

Fine root morphology

We separated the rhizomes of *L. chinensis* from their fine roots. We then carefully brushed the fine roots to remove soil so we could identify living and dead roots. We removed the dead roots and rinsed the living roots, and then determined their fresh weight. We then used a flatbed scanner (400 dpi resolution; DS-6500; Seiko Epson, Nagano, Japan) to scan the roots. We measured the total root length using the WinRHIZOPro root analysis program (Version 2004a; Regent Instruments Inc., Quebec City, QC, Canada). We then severed the roots at 5 cm below the ground surface (since more than 72% of belowground-biomass was found in the top 10 cm of the soil and total P concentration in 0–5 cm soil layer was 15.9–183% higher than that in 5–10 cm soil layer) and measured the root length in this near-surface (topsoil, 0–5 cm) and the total root length. We measured root shallowness as the root length in the topsoil layer divided by the total root length (RL_S/RL_T). We then calculated the specific root length (*SRL*, the length per unit dry mass).

Nutrient concentrations and stoichiometry, and nutrient resorption efficiency

We dried 200-mg samples of mature leaves and fresh leaf litter of *C. aristatum* and *L. chinensis* for 48 h at 65 °C, then ground them into a powder with a grinder. 0.2 g of powder was placed into a polytetrafluoroethylene digestion vessel with 2 mL of nitric acid. After cold digestion for 4 h, liquid was transferred to a stainless steel jacketed vessel. Then the vessel was placed in an oven at 165 °C for 4 h. After cooling, we diluted the liquid with ultrapure water to a volume of 10 mL. Then the P and Manganese (Mn) concentration of these samples were determined by inductively coupled plasma optical-emission spectroscopy (ICP-OES; OPTIMA 3300 DV, Perkin-Elmer Inc., Waltham, MA, USA). Manganese concentration of mature leaves has been used as a proxy for the rhizosphere carboxylic acid concentration (Pang et al. 2018). We measured the carbon (C) and nitrogen (N) concentrations using an elemental analyzer (CN802, VELP Scientifica Srl, Usmate Velate, Italy). We then calculated the mature leaf C: N: P.

We computed photosynthetic P- and N-use efficiency (*PPUE* and *PNUE*, respectively; Onoda et al. 2004) and P and N resorption efficiency (*PRE* and *NRE*, respectively; Du et al. 2020) as follows:

$$PPUE(\text{or } PNUE) = \frac{A_{max} \times SLA}{C_{ML}} \quad (12)$$

$$PRE(\text{or } NRE) = \frac{C_{ML} - C_{FLL}}{C_{ML}} \times 100\% \quad (13)$$

where C_{ML} is the P or N concentration in mature leaves and C_{FLL} is the P or N concentration in fresh leaf litter.

Soil properties, microbial biomass C: N:P, phosphatase activity, and microbial PLFAs

We weighed 15-g samples of fresh soil and then oven-dried the samples at 105 ℃ for 48 h to calculate the soil moisture content as [(Fresh weight – Dry weight)/Dry weight]×100%. Soil Olsen [P] was determined following the method of Yu et al. (2020) using a spectrophotometer (UH5300; Hitachi, Tokyo, Japan), with absorption at 882 nm. Soil pH was determined in suspension (soil: water, 1: 2 w/w) with a glass electrode. We determined microbial biomass C (*MBC*) and N (*MBN*) by the method of Vance (1987), and microbial biomass P (*MBP*) by the method of Brookes et al. (1982). We then calculated*MBC*/*MBP*, *MBC*/*MBN*, and *MBN*/*MBP*. We measured the V_{apmax} (maximum reaction velocity) for acid phosphatase activity (*AP*) then calculated the specific enzyme activity ($V_{apmax(s)}$) by dividing V_{apmax} by *MBC*, following the method of Raiesi and Beheshti (2014). We determined the relative P limitation parameter as 1-(*NRE*/*PRE*), where 1-(*NRE*/*PRE*) < 0 indicates that the plant was more limited by P than N, and defined the external P-acquisition parameter as $V_{apmax(s)}$ (Peng et al. 2023; Raiesi and Beheshti 2014). We also determined internal relative P abundance parameter as (*NRE*/*PRE*)-1.

We extracted the soil PLFAs using the improved method of Bossio and Scow (1998). The PLFAs were extracted from fresh soil with a 0.05 M dipotassium phosphate buffer to trichloromethane to methyl alcohol solution at a ratio of 5:6:12 (v/v/v) followed by centrifugation at 1041*g* for 10 min. Total, bacterial (*Bac*), fungal (*Fun*), arbuscular mycorrhizal fungal (AMF), actinomycete (*Act*), and eukaryote (*Euk*) PLFAs were determined with version 6.51 of the MIDI Sherlock Microbial Identification System (MIDI Inc., Newark, DE, USA) using a gas chromatograph (7890a; Agilent Technologies, Santa Clara, CA, USA).

Statistical analyses

Statistical analyses were conducted with version 22.0 of the SPSS software (SPSS Inc., Chicago, IL, USA). When the variance was homogeneous, one-way ANOVAs followed by LSD tests were performed to test the effects of five P-addition levels on traits of different species, and when the variance was heterogeneous, Welch's ANOVA followed by Games-Howell tests were performed. We checked percent-percent plots for normality using the Kolmogorov–Smirnov test before analysis, and all datasets were normally distributed. Differences were identified as significant at $p < 0.05$. We examined the relationships between P-addition level with Shannon-Wiener index, Simpson index, and Pielou's *E*, *AGB* of *C. aristatum* with *AGB* of *L. chinensis*, and Height similarity with *NO* using linear regression models.We used version 4.1.2 of the R software (https://www.r-project.org/) to perform linear regressions and calculate correlations between variables and to perform principal components analysis (PCA). We used Spearman's correlation coefficient (*r*) to quantify the strength of the correlations between traits. We used PCA to analyze the above- and belowground morphological and physiological changes that affected the niche characteristics of *C. aristatum and L. chinensis* at different P-addition level.

Results

Niche characteristics

Along the P-addition gradient, *Chenopodium aristatum*, *Chenopodium glaucum*, *Stipa grandis*, and *Medicago sativa* presented niche optima at the highest level ($P_{12.5}$; 64.0 mg kg^{-1} Olsen [P]); *Melilotoides ruthenicus*, *Thalictrum petaloideum*, *Cleistogenes squarrosa*, *Salsola collina*, and *Convolvulus ammannii* presented niche optima at the lowest level (Control; 5.18 mg kg^{-1} Olsen [P]); while *Leymus chinensis*, *Carex breviculmis* and *Artemisia frigida* had niche optima ranging from 21.6 to 44.8 mg kg^{-1} Olsen [P] (Figs. 1a, S4). *Leymus chinensis* had niche optima at 21.6 mg kg^{-1} Olsen [P] and showed the highest niche width among 12 species (Figs. 1a, S4). Niche overlap (*NO*) of *C. aristatum* and *L. chinensis* increased significantly, reaching its peak at $P_{2.5}$, then decreased, but the decrease was not significant (Fig. 1b).

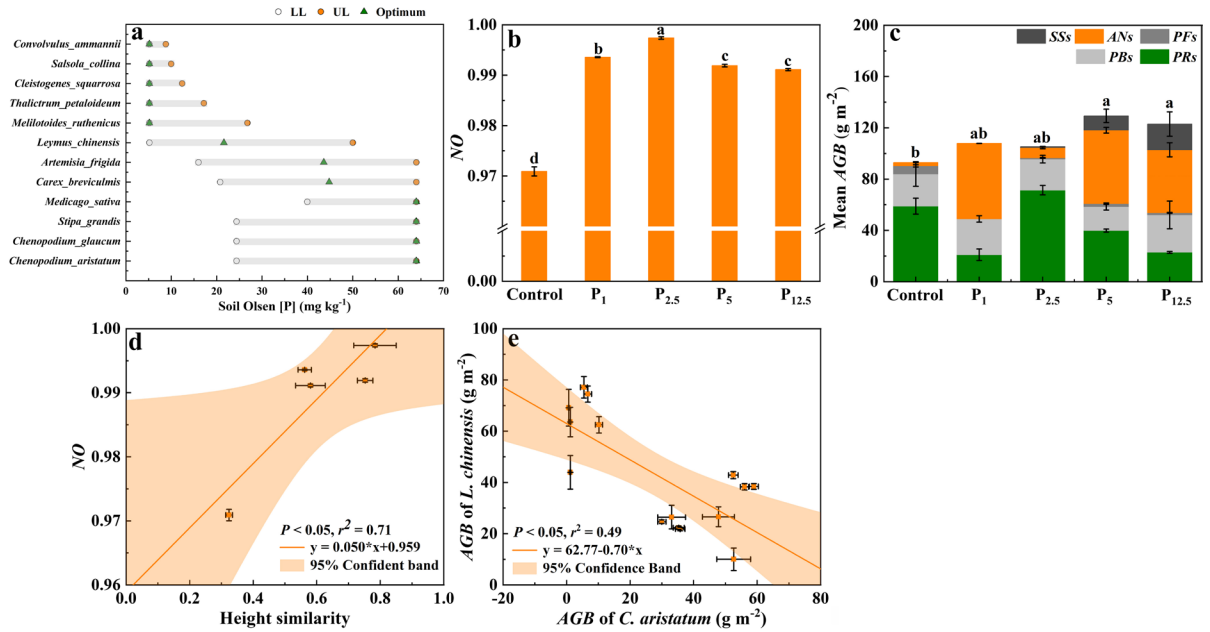

Fig. 1 **a** Modelled realized niches sorted by niche optima along soil available P gradient (5.18–64.00 mg kg^{-1}) by generalized additive models (GAMs) for 12 species under P-addition gradient. Green triangles are the niche optima of species determined by the gradient value of the relative density. Grey straight lines are the niche widths calculated by the difference between the borders of area of 80% under GAM-curve, and empty dots and orange dots are the lower limits (LL) and upper limits (UL), respectively. **b** Niche overlap (*NO*) of *Chenopodium aristatum* and *Leymus chinensis* (n = 3) and (**c**) aboveground biomass (*AGB*) of functional groups (n = 9) of the grassland communities under different P-addition levels: P_1, $P_{2.5}$, P_5, and $P_{12.5}$ represent P addition at 1, 2.5, 5, and 12.5 g P m^{-2} $year^{-1}$, respectively. Trait abbreviations as in Table S1. The values are means ± SE. Values of a parameter labeled with different lowercase and capital letters differ significantly between P addition levels for a given species and between species at a given P level, respectively ($p < 0.05$). **d** *NO* plotted against the height similarity of *C. aristatum* and *L. chinensis*. **e** *AGB* of *L. chinensis* plotted against *AGB* of *C. aristatum*

Importance values and biomass for the functional groups and community diversity

The importance values (*IV*) of different species and functional groups differed significantly among P-addition levels (Table S2). The *IV* of perennial rhizome grasses (*PRs*) and perennial bunchgrasses (*PBs*) were the highest among all functional groups in the control and at $P_{2.5}$ and P_5, whereas the *IV* of annuals (*ANs*) was highest at P_1 and $P_{12.5}$. *IV* of the *PRs* decreased significantly at P_1 and $P_{12.5}$, whereas the *IV* of *PBs* did not change with increasing P addition, except for a significant decrease at P_1 for *S. grandis*. The *IV* of perennial forbs (*PFs*) generally decreased significantly at all P-addition levels, but especially at P_1. The *IV* of all *ANs* increased significantly at P_1 (to 171.7% of the corresponding value in the control) and $P_{12.5}$. The sub-shrubs (*SSs*) functional group only showed a non-zero *IV* at P_5 and $P_{12.5}$.

Mean aboveground biomass (*AGB*) of the community increased with increasing P addition, reaching its peak value of 129 g m^{-2} at P_5, and then decreased, but not significantly (Fig. 1a). The *AGB* of the *PRs* accounted for 63, 20, 68, 31, and 19% of community aboveground biomass in the control at P_1, $P_{2.5}$, P_5, and $P_{12.5}$, respectively; in contrast, *AGB* of the *PBs* showed no significant difference among the P-addition levels. *AGB* of the *PFs* decreased significantly under P addition, whereas *AGB* of the *ANs* increased significantly, especially at P_1. Mean aboveground biomass (*AGB*) of *C. aristatum* was significantly negatively correlated with *AGB* of *L. chinensis* ($P < 0.05$, $r = -0.7$; Fig. 1e).

Community diversity and evenness differed significantly among P-addition levels, though the pattern differed among indices (Fig. S1). The Shannon-Wiener index and Pielou's *E* was significantly positively correlated with P-addition level ($P < 0.05$; Fig. S1a,

c), whereas the Simpson index showed no significant correlation with P-addition level (Fig. S1b).

Aboveground morphological similarity and growth rates

Vegetation cover, plant height, and leaf area (*LA*) of *C. aristatum* increased significantly with increasing P addition, whereas the vegetation cover and plant height of *L. chinensis* showed no significant difference from the control and its *LA* only increased significantly at $P_{2.5}$ (Fig. 2a-c). Morphological similarities differed under the P-addition levels (Fig. S2). The height similarity increased significantly with increasing P addition, reaching a peak at $P_{2.5}$, and leaf area similarity increased significantly at P_1, P_5, and $P_{12.5}$. Height similarity increased significantly with increasing *NO* of *L. chinensis* and *C. aristatum* ($p < 0.05$, $r^2 = 0.71$; Fig. 1f).

Specific leaf area (*SLA*) of *C. aristatum* decreased significantly at P_5 and $P_{12.5}$, whereas SLA of *L. chinensis* decreased significantly only at $P_{2.5}$ (Fig. 2d). The aboveground growth rate (*AGR*) of *C. aristatum* increased significantly at P_1, P_5, and $P_{12.5}$, whereas *AGR* of *L. chinensis* decreased significantly at P_1 and increased significantly at $P_{2.5}$ (Fig. 2e). The *AGR* of *C. aristatum* was significantly greater than that of *L. chinensis*, except in the control and at $P_{2.5}$.

Leaf nutrient status and nutrient-resorption efficiency

Leaf nutrient status and nutrient-resorption efficiency responded differently to the P-addition levels (Fig. 3). Leaf [P] of *C. aristatum* increased significantly at all P-addition levels, whereas leaf [P] of *L. chinensis* only increased significantly at $P_{2.5}$, P_5, and $P_{12.5}$ (Fig. 3a). Leaf [N] of *C. aristatum* decreased significantly at P_5 and $P_{12.5}$, whereas leaf [N] of *L. chinensis* showed no significant response to P addition (Fig. 3b). *PRE* of *C. aristatum* did not differ significantly among P-addition levels, except for a significant decrease at $P_{12.5}$, whereas *PRE* of *L. chinensis* decreased significantly at P_5 and $P_{12.5}$ (Fig. 3c). Nitrogen-resorption efficiency (*NRE*) of *C. aristatum* increased significantly at all P-addition levels, whereas *NRE* of *L. chinensis* increased significantly at $P_{2.5}$, P_5 and $P_{12.5}$ (Fig. 3d). Phosphorus-resorption efficiency (*PRE*) and *NRE* of *C. aristatum* were significantly greater than those of

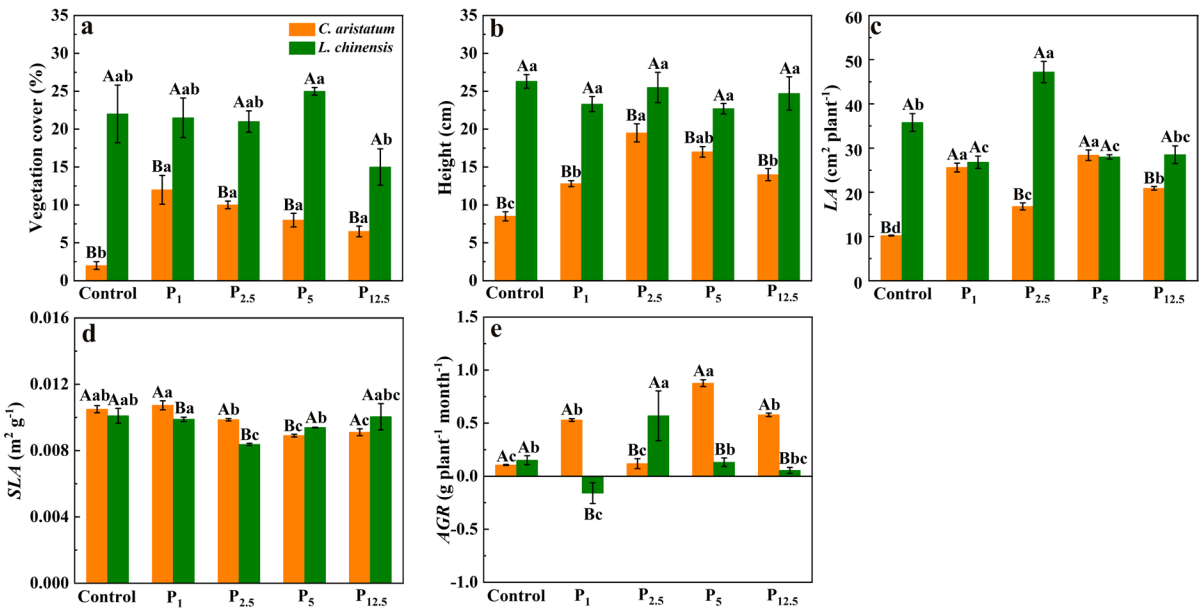

Fig. 2 **a** Vegetation cover, **b** height, **c** leaf area (*LA*), **d** specific leaf area (*SLA*), and (**e**) aboveground growth rate (*AGR*) of *Chenopodium aristatum* and *Leymus chinensis* under different P-addition levels: P_1, $P_{2.5}$, P_5, and $P_{12.5}$ represent P addition at 1, 2.5, 5, and 12.5 g P m^{-2} $year^{-1}$, respectively. Trait abbreviations as in Table S1. The values are means (SE) ($n = 9$). Values of a parameter labeled with different lowercase and capital letters differ significantly between P addition levels for a given species and between species at a given P level, respectively ($p < 0.05$)

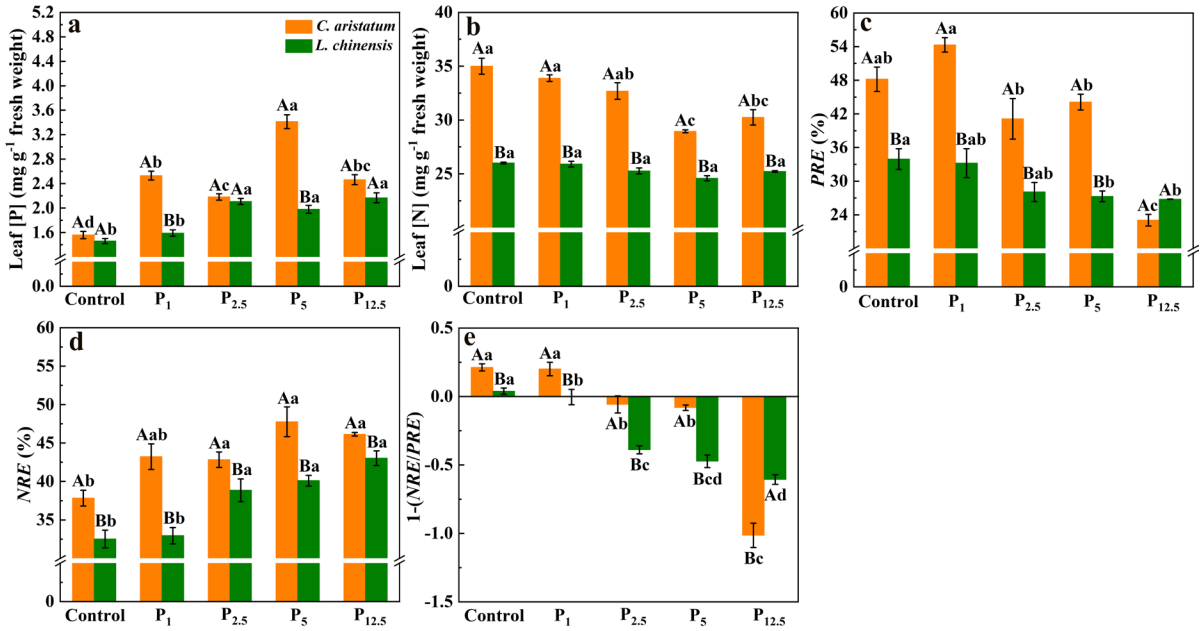

Fig. 3 Leaf (**a**) phosphorus concentration ([P]) and (**b**) nitrogen concentration ([N]), and the (**c**) phosphorus-resorption efficiency (*PRE*) and (**d**) nitrogen-resorption efficiency (*NRE*), and (**e**) the relative P limitation (1-(*NRE*/*PRE*)) of *Chenopodium aristatum* and *Leymus chinensis* under different P-addition levels. P_1, $P_{2.5}$, P_5, and $P_{12.5}$ represent P addition at 1, 2.5, 5, and 12.5 g P m^{-2} $year^{-1}$, respectively. Trait abbreviations as in Table S1. The values are means (SE) ($n = 9$). Values of a variable labeled with different lower-case and capital letters differ significantly between P-addition levels for a species and between species at a given P level, respectively ($p < 0.05$)

L. chinensis at all P-addition levels. The relative P limitation of *C. aristatum* and *L. chinensis* decreased significantly with increasing P addition, and the relative P limitation of *C. aristatum* was significantly more severe than that of *L. chinensis*, except at $P_{12.5}$ (Fig. 3e).

Photosynthetic parameters, fluorescence parameters, intrinsic water-use efficiency, and photosynthetic N- and P-use efficiency

The photosynthetic parameters, fluorescence parameters and total chlorophyll per unit leaf area (Chl_{Total}) of *C. aristatum* and *L. chinensis* differed significantly among P-addition levels (Fig. 4). The net photosynthetic rate (*A*) of *C. aristatum* increased significantly with increasing P addition, especially at P_1, whereas the *A* of *L. chinensis* increased significantly only at $P_{2.5}$ (Fig. 4a). The maximum photosynthetic rate (A_{max}), maximum carboxylation efficiency (V_{cmax}), and maximum electron-transport rate (J_{max}) of *C. aristatum* increased significantly at P_1, whereas V_{cmax} and J_{max} of *L. chinensis* increased significantly at $P_{2.5}$ and P_5 (Fig. 4b, d, e). The light-saturation point (*LSP*) of *C. aristatum* increased significantly only at $P_{2.5}$ and P_5, while *LSP* of *L. chinensis* increased significantly under P addition (Fig. 4c). Intrinsic water-use efficiency (*iWUE*) of *C. aristatum* increased significantly at all P-addition levels, whereas *iWUE* of *L. chinensis* increased significantly at $P_{2.5}$ and P_5 (Fig. 4f). The maximum quantum efficiency of PSII (F_v/F_m) and energy-harvesting efficiency of PSII (F_v'/F_m') of *C. aristatum* showed no significant difference from the control under P addition, while for *L. chinensis*, F_v/F_m, F_v'/F_m' and Chl_{Total} increased significantly at $P_{2.5}$ or $P_{12.5}$ or at both levels (Fig. 4g, h). The total chlorophyll concentration per unit leaf area of *C. aristatum* increased significantly at P_1, but decreased significantly at $P_{12.5}$; Chl_{Total} of *L. chinensis* increased at $P_{2.5}$ (Fig. 4i). Photosynthetic P-use efficiency (*PPUE*) of both species decreased significantly at all P-addition levels (Fig. 4j, k). Photosynthetic N-use efficiency (*PNUE*) of *C. aristatum* increased significantly at P_1, $P_{2.5}$, and P_5, whereas *PNUE* of *L. chinensis* showed no

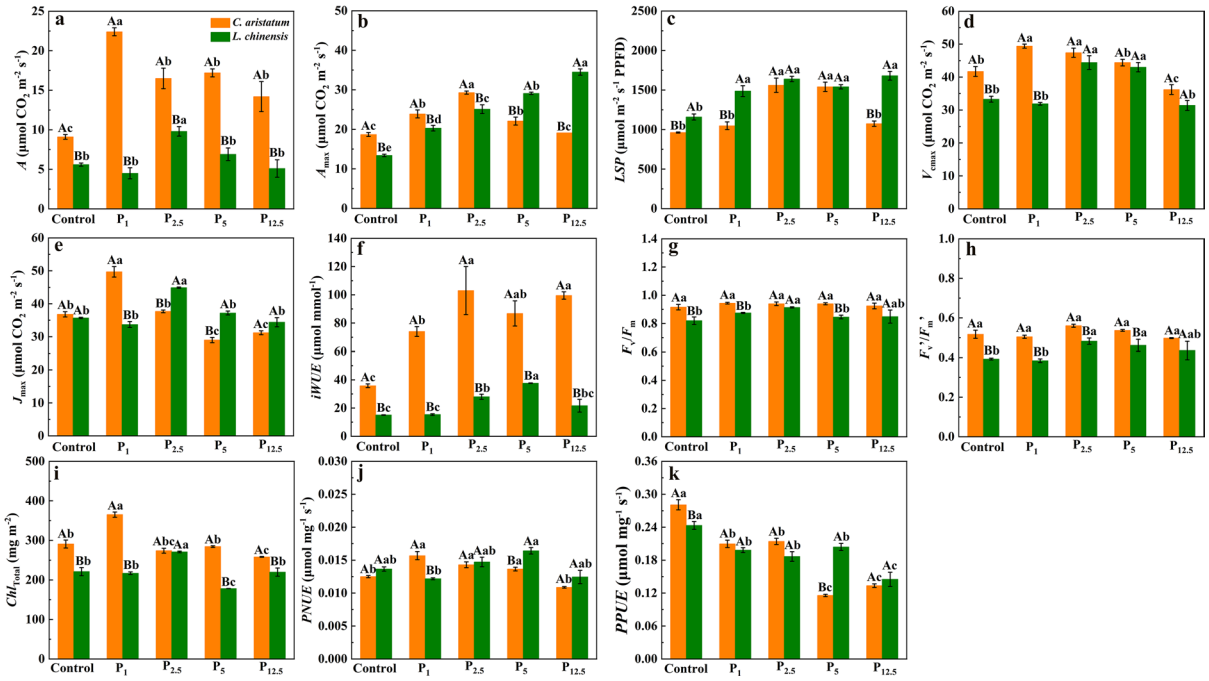

Fig. 4 **a-e** Photosynthetic characteristics, **f** intrinsic water-use efficiency (*iWUE*), **g-h** chlorophyll fluorescence parameters, **i-j** photosynthetic nitrogen (N)- and phosphorus (P)-utilization efficiency (*PNUE* and *PPUE*), and (**k**) total chlorophyll per unit leaf area (Chl_{Total}) of *Chenopodium aristatum* and *Leymus chinensis* under different P-addition levels: P_1, $P_{2.5}$, P_5, and $P_{12.5}$ represent P addition at 1, 2.5, 5, and 12.5 g P m^{-2} $year^{-1}$, respectively. Trait abbreviations as in Table 1. The values are means (SE) ($n = 9$). Values of a variable labeled with different lower-case and capital letters differ significantly between P-addition levels for a species and between species at a given P level, respectively ($p < 0.05$)

significant response to P addition. Net photosynthetic rate, F_v/F_m, F_v'/F_m', and *iWUE* of *C. aristatum* were generally higher than those of *L. chinensis*.

For *C. aristatum*, *AGB* was significantly positively correlated with leaf [P] and *NRE* (Fig. 5a). Plant height was significantly positively correlated with *LSP* and *iWUE*, and vegetation cover was significantly positively correlated with *A*, A_{max}, V_{cmax}, and F_v/F_m. For *L. chinensis*, *AGB* and *AGR* was significantly positively correlated with *A* and J_{max} (Fig. 5b). In addition, height was significantly positively correlated with Chl_{Total}, and vegetation cover was significantly positively correlated with *PPUE*.

Belowground morphology and architecture

The belowground morphology and architecture of *C. aristatum* and *L. chinensis* differed significantly among the P-addition levels (Fig. 6). Root diameter (*RD*) of *C. aristatum* decreased significantly, whereas *RD* of *L. chinensis* showed no significant change under P addition (Fig. 6a). Specific root length (*SRL*) of *C. aristatum* increased significantly under P addition, whereas *SRL* of *L. chinensis* generally decreased significantly, except for an increase at $P_{12.5}$ (Fig. 6b). Root shallowness (RL_S/RL_T) of *C. aristatum* showed no significant change under P addition, whereas RL_S/RL_T of *L. chinensis* increased significantly at P_1, but decreased significantly at P_5 and $P_{12.5}$ (Fig. 6c). Root: shoot ratio of *C. aristatum* decreased significantly at P_5 and $P_{12.5}$, while R/S of *L. chinensis* showed no significant change under P addition (Fig. 6d). Leaf [Mn] of *C. aristatum* decreased significantly at all P-addition levels, whereas leaf [Mn] of *L. chinensis* increased significantly at $P_{2.5}$, P_5, and $P_{12.5}$ (Fig. 6e). Root diameter of *L. chinensis* was significantly higher than that of *C. aristatum*, whereas *SRL* and leaf [Mn] of *C. aristatum* was significantly higher than that of *L. chinensis*.

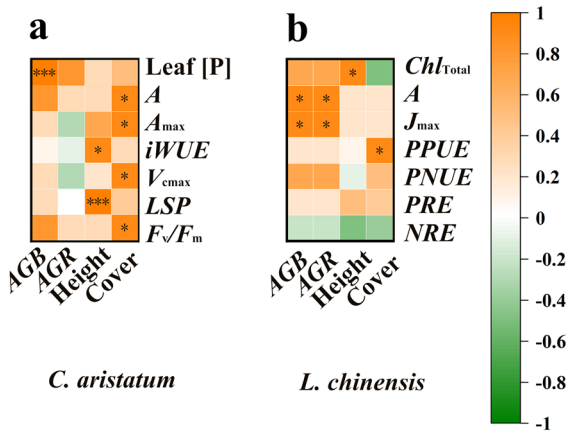

Fig. 5 Spearman's correlations (*r*) among aboveground biomass (*AGB*), aboveground growth rate (*AGR*), height, vegetation cover, leaf phosphorus (P) concentration ([P]), total chlorophyll per unit leaf area (Chl_{Total}), net photosynthetic rate (*A*), maximum photosynthetic rate (A_{max}), intrinsic water-use efficiency (*iWUE*), maximum carboxylation efficiency (V_{cmax}), maximum electron transport rate (J_{max}), Light-saturation point (*LSP*), maximum quantum efficiency of PSII (F_v/F_m), photosynthetic nitrogen (N)- and phosphorus (P)-utilization efficiency (*PPUE* and *PNUE*), phosphorus-resorption efficiency (*PRE*) and (d) nitrogen-resorption efficiency of (**a**) *Chenopodium aristatum* and (**b**) *Leymus chinensis* under different P-addition levels. Trait abbreviations as in Table S1. Significance: $*p<0.05$, $**p<0.01$, and $***p<0.001$

Biochemical traits in the rhizosheath and bulk soil

The chemical traits of the rhizosheath and bulk soil differed among P-addition levels. Olsen [P] and pH increased significantly with increasing P addition for both species, and the increase of Olsen [P] in the rhizosheath soil was greater than that in the bulk soil, especially for the rhizosheath of *C. aristatum* (Fig. 7a, b). The topsoil (0 to 5 cm) showed higher Olsen [P] but a lower moisture content than the subsoil did (5 to 10 cm; Table S3). Acid phosphatase activity (*AP*) decreased with increasing P addition, and the difference became significant at P_1 or $P_{2.5}$ and the decrease of *AP* in the bulk soil was greater than that in the two rhizosheath soils (Fig. 7d). The decrease of specific *AP* ($V_{apmax\ (s)}$) in the rhizosheath soil of *C. aristatum* was generally greater than that of *L. chinensis* (Table S4).

Microbial biomass and its compositions in the rhizosheath and bulk soil responded differently to P addition (Figs. 7e, f, S3). The concentration of total phospholipid fatty acids (PLFAs) increased significantly with increasing P addition in the rhizosheath of *C. aristatum*, whereas in the rhizosheath of *L. chinensis*, total PLFAs increased significantly, reaching a peak at $P_{2.5}$, and then decreased (Fig. S3a). The trends for bacterial (*Bac*), actinomycete (*Act*), and eukaryotic (*Euk*) PLFAs in the rhizosheaths of *C. aristatum* and *L. chinensis* were similar to the trends for total PLFAs (Figs. 7e, S3c, d). AMF and fungal (*Fun*) PLFAs in the bulk soil and the rhizosheath soil of *C. aristatum* decreased with increasing P addition, whereas AMF and fungal PLFAs in the rhizosheath soil of *L. chinensis* increased under P addition, especially at $P_{2.5}$.

Trade-offs between internal and external P strategies, plant–microbe stoichiometry, and differential responses of above- and belowground characteristics

For both *C. aristatum* and *L. chinensis*, there were significant negative correlations between internal relative P abundance and external P-acquisition parameters along the P-addition gradient (Fig. 8a, b). For *C. aristatum*, there was no significant correlation between leaf and soil C: N: P stoichiometry (Fig. 8c), whereas for *L. chinensis*, there was a significant positive correlation between the leaf C: P ratio and the rhizosheath *MBC: MBP* ratio (Fig. 8d).

For *C. aristatum*, we found that principal components analysis (PCA) axes 1 and 2 accounted for 82.3 and 86.4%, respectively, of the variation for above- and belowground traits. For *L. chinensis*, we found that PCA axes 1 and 2 accounted for 74.7 and 98.3%, respectively, of the variation for above- and belowground traits. Based on our PCA, we found differential responses of above- and belowground characteristics along the P-addition gradient (Fig. 9). For the aboveground traits of *C. aristatum*, PCA 1 and PCA 2 distinctly separated *C. aristatum* at P_1 and P_5 from the other P levels and were associated with a higher *A* (Fig. 9a); for the aboveground traits of *L. chinensis*, PCA 1 and PCA 2 distinctly separated *L. chinensis* at $P_{2.5}$ from the other P levels, with a higher J_{max}, Chl_{Total}, *AGR*, *AGB*, F_v'/F_m', and *A* (Fig. 9c). For the belowground traits of *C. aristatum*, PCA 1 and PCA 2 distinctly separated *C. aristatum* at P_1 and P_5 from the other P levels, with a higher *AGB*, and *AGR* (Fig. 9b), whereas for belowground traits of *L. chinensis*, PCA 1 and PCA 2 distinctly separated *L.*

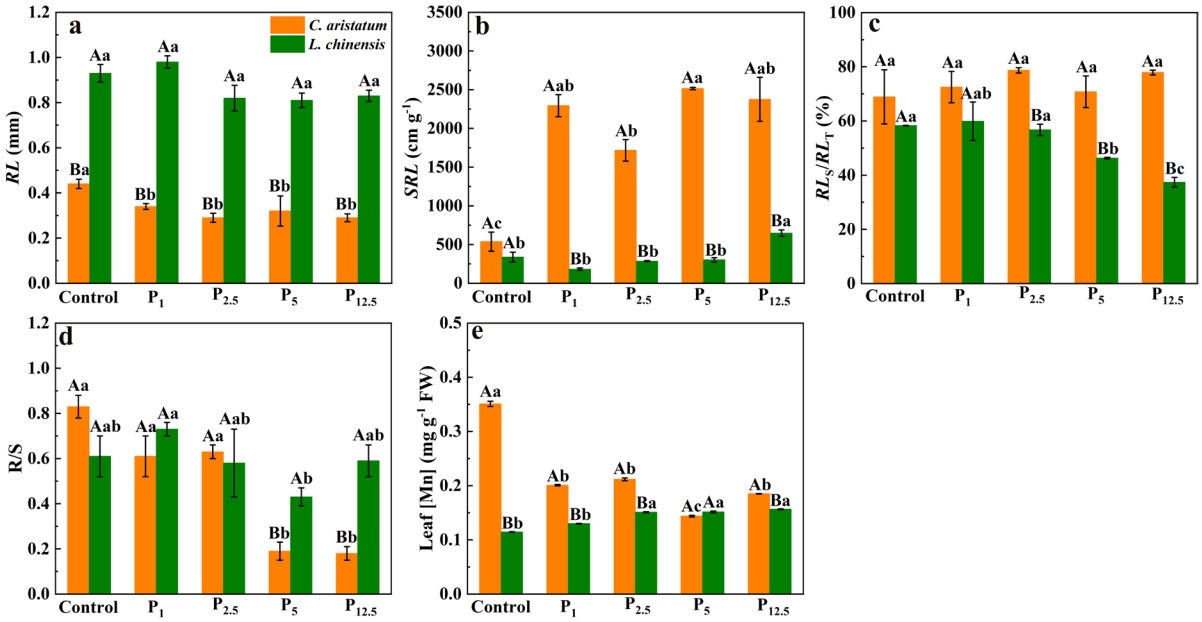

Fig. 6 **a** Root diameter (*RD*), **b** specific root length (*SRL*), **c** root shallowness (RL_S/RL_T), **d** the root to shoot ratio (R/S), and (**e**) the rhizosphere carboxylic acid concentration (proxied by leaf [Mn]) of *Chenopodium aristatum* and *Leymus chinensis* under different phosphorus (P)-addition levels: P_1, $P_{2.5}$, P_5, and $P_{12.5}$ represent P addition at 1, 2.5, 5, and 12.5 g P m^{-2} $year^{-1}$, respectively. Trait abbreviations as in Table S1. The values are means (SE) ($n = 9$). Values of a variable labeled with different lower-case and capital letters differ significantly between P-addition levels for a species and between species at a given P level, respectively ($p < 0.05$)

chinensis at $P_{2.5}$ from the other P levels, with a higher *AGR*, *AGB*, *Act*, *AMF*, *Fun*, and *Euk* (Fig. 9d).

Discussion

Responses to P addition along the aboveground niche axes

Phosphorus addition changes community productivity and stability by altering the community's functional composition (García-Palacios et al. 2018; Ávila-Lovera et al. 2021). In the present study, both aboveground biomass and diversity increased with increasing P addition. This reveals that interspecific competition intensified under P addition (Fornara and Tilman 2009; Liu et al. 2018). Dominance of*L. chinensis* (the dominant species at our study site, a perennial mycorrhizal C_3grass) strongly improves grassland stability in northern China (Cohen 1994; Li et al. 2019). However, the importance value of a competing forb (*C. aristatum*, an annual non-mycorrhizal C_4 forb) greatly increased under P fertilization and this species occupied some of the niche of *L. chinensis*, especially under low P addition (P_1). We observed significant loss of aboveground biomass by *L. chinensis*, except under medium P addition ($P_{2.5}$). Remarkably, under relatively high and high P addition (P_5 and $P_{12.5}$), competition between *C. aristatum* and *L. chinensis* decreased slightly; the total aboveground biomass of the community increased, and surplus niches were mainly occupied by an invasive subshrub (*A. frigida*). These results indicate the occurrence of reverse succession at P_5 and $P_{12.5}$ (Li et al. 2019). The competition between*C. aristatum* and *L. chinensis* might therefore lead to a decreasing community stability at P_1, P_5, and $P_{12.5}$ (Harpole and Suding 2011; Ren et al. 2016).

The plant–plant interactions that occur under P fertilization depend on morphological and physiological changes (Happonen et al. 2022). The vegetation cover, plant height, and leaf area (*LA*) of *C. aristatum* increased sharply under P addition (vegetation cover increased by up to 500% at P_1 and up to 225% at $P_{12.5}$), and aboveground growth rate (*AGR*) was enhanced at P_1, P_5, and $P_{12.5}$. These

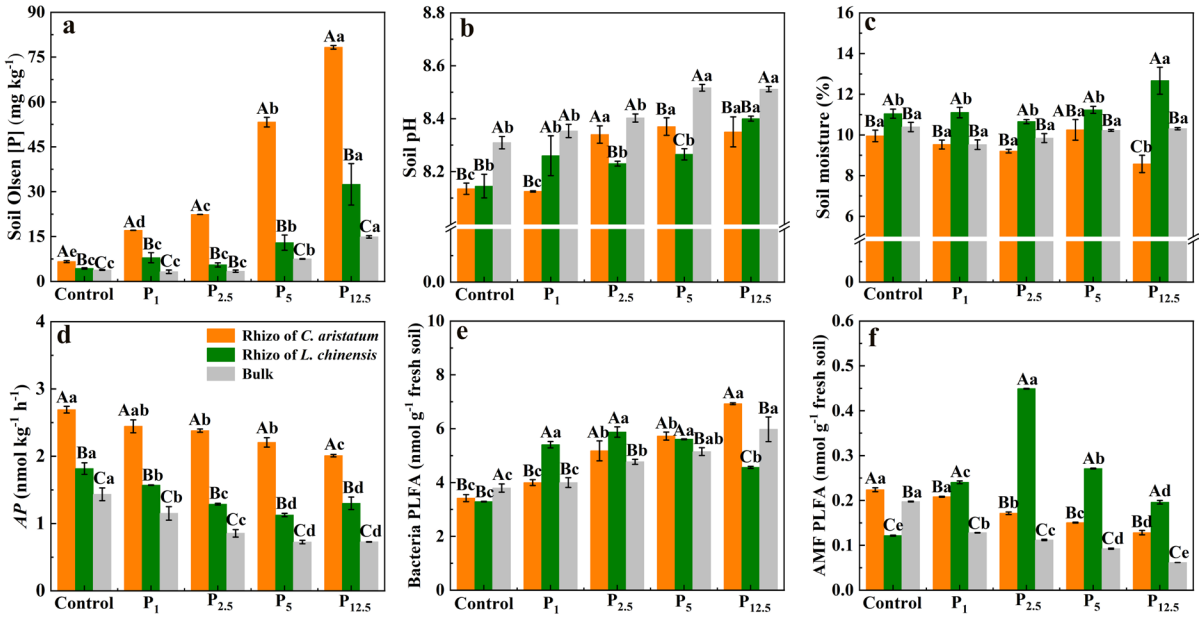

Fig. 7 Soil (**a**) Olsen phosphorus (P) concentration ([P]), (**b**) pH, (**c**) soil moisture, (**d**) acid phosphatase activity (*AP*), and the concentrations of (**e**) bacterial and (**f**) AMF phospholipid fatty acids for the *Chenopodium aristatum* and *Leymus chinensis* rhizosheaths and in the bulk soil under different P-addition levels: P_1, $P_{2.5}$, P_5, and $P_{12.5}$ represent P addition at 1, 2.5, 5, and 12.5 g P m^{-2} $year^{-1}$, respectively. Trait abbreviations as in Table S1. The values are means ± SE ($n = 9$). Values of a parameter labeled with different lowercase letters differ significantly ($p < 0.05$) among P-addition levels for a given species or bulk soil; different capital letters represent significant differences between the species or bulk soil at a given P addition

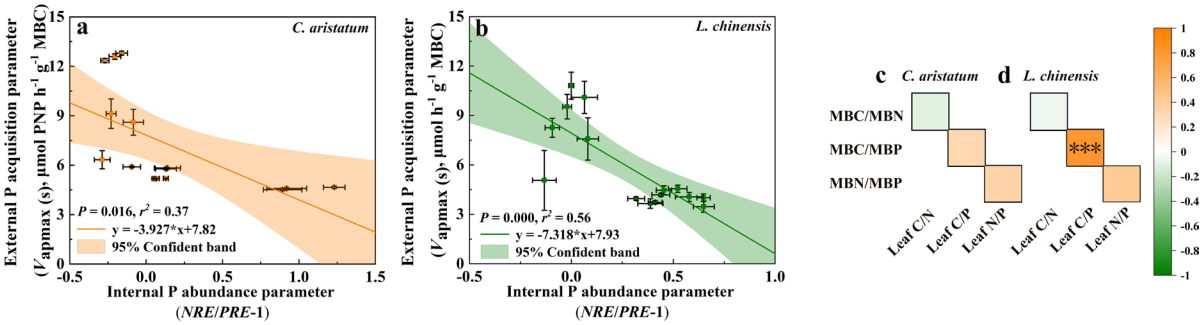

Fig. 8 Correlations between the internal relative Phosphorus abundance parameter ((*NRE*/*PRE*)-1; *NRE*: nitrogen-resorption efficiency; *PRE*: phosphorus-resorption efficiency) and the external P-acquisition parameters ($V_{apmax\ (s)}$: specific acid phosphatase activity) of (**a**) *Chenopodium aristatum* and (**b**) *Leymus chinensis*. Spearman's correlations (r) among leaf, fine root, and rhizosheath soil microbial biomass C: N:P stoichiometry for (**c**) *C. aristatum* and (d) *L. chinensis* under different P-addition levels. Trait abbreviations as in Table 1. Significance: *$p < 0.05$, **$p < 0.01$, and ***$p < 0.001$

changes might greatly increase biomass accumulation and competitiveness of this species (Baldarelli et al. 2021). Increased morphological similarity increases niche overlap, which might lead to competitive exclusion (Huang et al. 2022). Height similarity and niche overlap (*NO*) were significantly positively correlated under P addition. This indicates that greater height plasticity triggered by P addition might exacerbate interspecific competition (Díaz et al. 2006; Huang et al. 2022). Specific leaf area (*SLA*) is a functional indicator of the leaf area that intercepts the light (Shipley 2006). The*SLA* of *C. aristatum* decreased at P_5 and $P_{12.5}$. This means that *C. aristatum* tended to adopt a more conservative

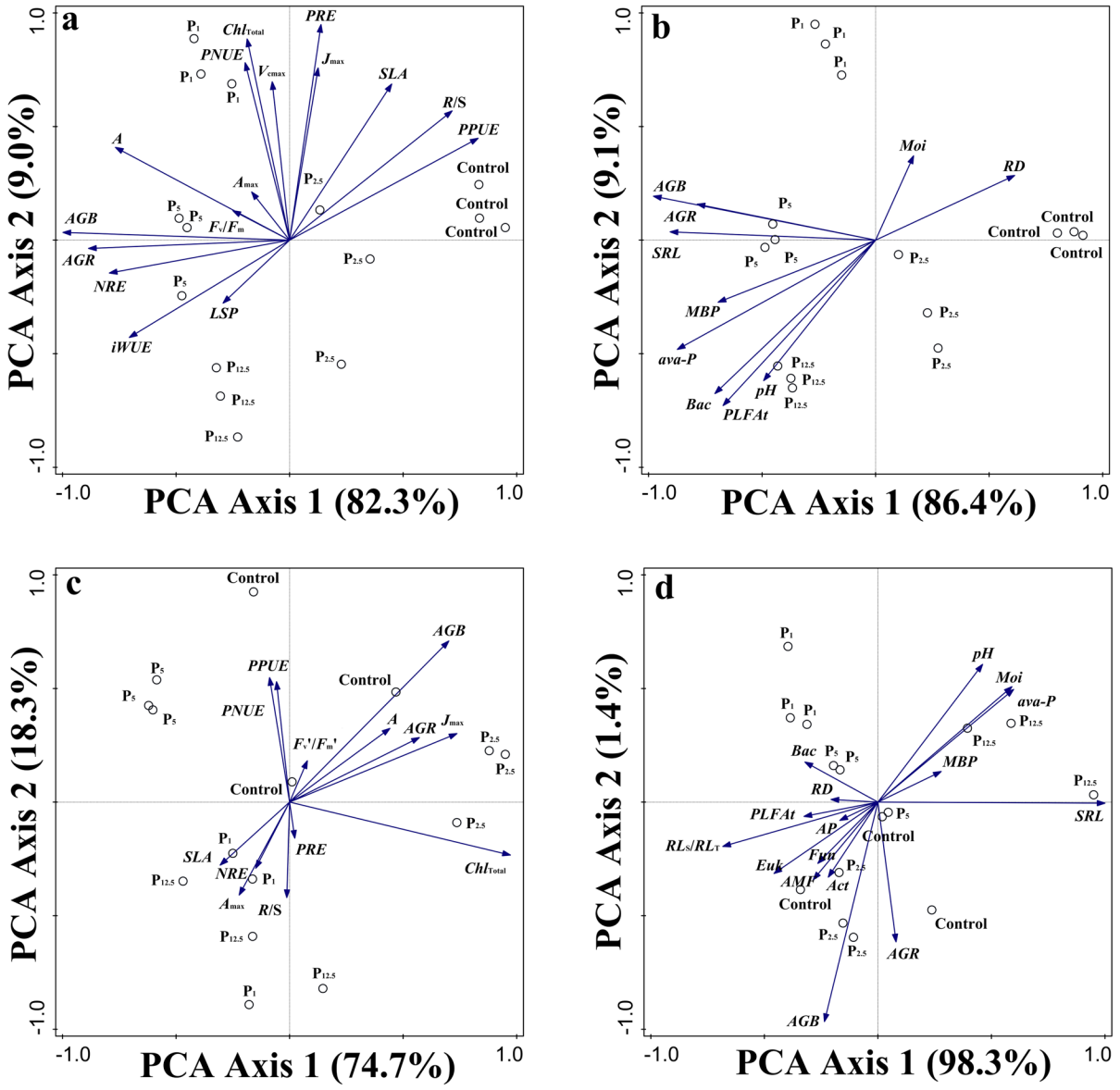

Fig. 9 Principal components analysis (PCA) biplots for the first two PCA axes for (**a**) aboveground and (**b**) belowground traits of *Chenopodium aristatum* and (**c**) aboveground and (**d**) belowground traits of *Leymus chinensis* under different phosphorus-addition levels. P_1, $P_{2.5}$, P_5, and $P_{12.5}$ represent P addition at 1, 2.5, 5, and 12.5 g P m^{-2} $year^{-1}$, respectively. Trait abbreviations as in Table S1

foliar strategy, which would decrease competition for light at P_5 and $P_{12.5}$ (Krüger et al. 2017; Wright et al. 2005). In contrast, the plant morphology of*L. chinensis* showed no significant responses to P addition, and *AGR* increased only at $P_{2.5}$. This means that *L. chinensis*had specific traits to respond to soil P availability that enhanced its biomass accumulation (Shi et al. 2020).

Photosynthesis is the primary physiological process that assimilates CO_2, and P is an essential substrate and powerful regulator of photosynthesis (Mo et al. 2019; Sanaei and Ali 2019). C_4 plants such as *C. aristatum* have a higher intercellular CO_2 concentration, which enhances their rate and efficiency of carbon assimilation, but this function requires extra enzyme (PEP carboxylase) and more P (Levey et al.

2018; Yin and Struik 2011). Phosphorus addition sharply increased net photosynthetic rate (*A*) of *C. aristatum*, and this was associated with an increased maximum photosynthetic rate (A_{max}), maximum carboxylation rate (V_{cmax}), and maximum electro- transport rate (J_{max}). This means that P addition increased the assimilatory power of this species by enhancing CO_2- and light-utilization efficiency (Martini et al. 2019; Slot and Winter 2017). In addition, intrinsic water-use efficiency (*iWUE*) and light-saturation point (*LSP*) were positively correlated with plant height of *C. aristatum*. This indicates that the increase of plant height might be associated with increased light utilization and water conservation under P addition (Yan et al. 2013). The large increase of*A* at P_1 (by 135.8%) was associated with efficient functioning of photosystem II complexes (PSII), which sustained its maximum quantum efficiency (F_v/F_m) at around 0.90. This enhanced photophosphorylation of *C. aristatum* at P_1 (Zhou et al. 2015). Moreover, P_1 greatly increased its P status (its leaf [P] increased from 1.56 to 2.53 mg g^{-1}), as its leaf N: P ratio decreased from 22.4 to 13.3 (Güsewell 2004). In addition, at P_1 P- and N-resorption efficiency (*PRE* and *NRE*) were maintained, but it sharply increased leaf [P] (by 56.3%) and total chlorophyll per unit leaf area (Chl_{Total}; by 25.6%). These changes mean that *C. aristatum* was able to modify its foliar N and P economy, and thus to greatly increase photosynthesis at P_1 (Warren et al. 2000). Interestingly, at $P_{12.5}$, although the *A* of *C. aristatum* increased moderately (by 49.5%), its leaf [N], Chl_{Total}, and V_{cmax}decreased significantly. This suggests that when P addition exceeds a threshold, N simply became limiting, and hence leaf (Fiorentini et al. 2019; Su et al. 2021), which might result from inhibition of N uptake by microbes (which we will discuss further in "Belowground niche differences triggered by P addition" and "Trade-offs in plant–microbe feedbacks" sections). This severe N limitation would decrease Rubisco activity and chlorophyll synthesis, leading to decreased photosynthetic P-utilization rate (*PPUE*) of *C. aristatum* at $P_{12.5}$ (Smith 2022).

C_3 photosynthesis is less P-efficient than C_4photosynthesis (Ghannoum et al. 2008). For*L. chinensis*, leaf [P] and *A* showed no significant response to P_1, and this was associated with a low *PPUE*. This lack of a response indicates that a photosynthetic increase of *L. chinensis* required a larger P supply than was required by *C. aristatum* due to the lower P-use efficiency of C_3plants (Ghannoum and Conroy 2007). Net photosynthetic rate of*L. chinensis* increased greatly (by 75.0%) at $P_{2.5}$, whereas *A* did not increase further under higher P levels; V_{cmax} and J_{max} also peaked at $P_{2.5}$. These responses indicate that $P_{2.5}$ was more suitable for carbon assimilation of *L. chinensis* than lower or higher P levels. Moreover, *L. chinensis* maintained its leaf [N], even at $P_{12.5}$. This can be attributed to its responsive *NRE* (by 21.0% at $P_{12.5}$; Li et al. 2012; Yang 2018). However, this advantage of N conservation did not alleviate the loss of niches by*L. chinensis* at $P_{12.5}$, and belowground responses of this species might determine this niche dynamic (which we discuss further in "Belowground niche differences triggered by P addition" and "Trade-offs in plant–microbe feedbacks" sections).

In summary, these results support our hypothesis 1: *C. aristatum* will increasingly occupy the niche of *L. chinensis* under P addition and show more responsive photosynthetic characteristics.

Belowground niche differences triggered by P addition

Stable coexistence between competing species requires high functional diversity, and P addition can act as a trigger of niche differences (Jacoby and Kopriva 2019; Ma et al. 2018; Silvertown 2004). In our study, P addition promoted segregation of root depth, root morphology, and microbial mediation of*C. aristatum* and *L. chinensis*. Segregation of root architectures can be attributed to soil heterogeneity (Walk et al. 2006) as a function of depth, as the difference of the Olsen [P] values between the topsoil (0 to 5 cm) and subsoil (5 to 10 cm) increased from 1.1 mg/kg (in the control) to 44.3 mg/kg (at $P_{12.5}$). The root shallowness (RL_S/RL_T) of *L. chinensis* decreased significantly at P_5 and $P_{12.5}$, whereas that of *C. aristatum* was relatively steady at 68.9 to 78.7% along the P-addition gradient. These different responses lead to the separation of the root distribution range of *L. chinensis* and *C. aristatum* in the soil profile. These characteristics help increase root functional diversity, which was associated with slightly decreased *NO* at P_5 and $P_{12.5}$ (Aschehoug and Callaway 2014; Wijesinghe et al. 2005). Moreover, these changes might also promote differential water acquisition due to the

spatial separation of rainfall and deep-soil water (Li et al. 2009; Lynch and Brown 2008).

Root morphological variability under P addition greatly affects P acquisition, and thus changes the coexistence of annuals and perennials (Aschehoug and Callaway 2014; Kramer-Walter et al. 2016). The specific root length (*SRL*) of *C. aristatum* increased significantly under P addition. This reveals that its roots could occupy more belowground space per unit biomass invested, especially at P_1, P_5, and $P_{12.5}$, thus increasing belowground competition (Zhou et al. 2019). Moreover,*C. aristatum* had finer roots; its root diameter (*RD*) decreased, but its *SRL* increased under P addition. This suggests higher root morphological plasticity than in *L. chinensis*, which let *C. aristatum*promote its ability to take up nutrients, particularly in a fertile soil (Lynch and Ho 2005; Zhou et al. 2022). These changes were associated with increasing B_L of *C. aristatum*. In addition, the root system of this non-mycorrhizal species tends to obtain resources by itself, without relying on arbuscular mycorrhizal fungal (AMF) symbionts like most other species do (Ma et al. 2018). In contrast, *L. chinensis* had coarser roots, its *RD* did not change under P addition, and its *SRL* increased slightly only at $P_{12.5}$. These responses indicate that it tended to retain a relatively conservative functional type, which usually has a greater mycorrhizal colonization rate (Barazetti 2019; Ma et al. 2018). These results were supported by the increased AMF PLFAs that we observed in its rhizosheath under P addition.

Rhizosheath microbial mediation of nutrient uptake is an important factor that determines species coexistence under P addition (DeFores 2019; Moran 2017). In our study, soil acid phosphatase activity (*AP*) decreased with increasing P addition, but P addition increased the difference in plant-available soil P concentration (Olsen [P]) and *AP* between the bulk and rhizosheath soil. This indicates that increased soil P availability might be associated with decreased mineralization of organic P, and root exudates might partly alleviate this effect, thereby promoting plant coexistence (Liu et al. 2014; Shi et al. 2023; Zhu et al. 2020). High functional diversity of the microbial community is associated with high diversity of the microbial community composition, which is modified by P addition and plant–microbe interactions (Rejmánková and Sirová 2007; Strickland and Rousk 2010; Xiao et al. 2020). Phosphorus addition decreased the dominance of fungi and AMF, but increased the dominance of bacteria in the rhizosheath soil of *C. aristatum* and in the bulk soil. Moreover, the leaf [Mn] (a proxy for rhizosphere carboxylic acid concentrations) of *C. aristatum* decreased significantly with increasing P addition. These results indicate that it was the P addition level that determined the decrease of AMF biomass in the rhizosheath of *C. aristatum*, resulting in larger differences of the microbial community composition between the rhizosheath soil of *C. aristatum* and that of *L. chinensis* under P addition, thereby increasing functional diversity (Barazetti 2019; Lynch and Ho 2005; Pang et al. 2018; Tran et al. 2020; Ven et al. 2019).

Functional microbial mediation mitigates the negative effects of interspecific competition and promotes co-growth of above- and belowground organs (Smith 2011). In our study, *NO* peaked at $P_{2.5}$. However, the growth of *L. chinensis* increased significantly at $P_{2.5}$, which might depend on its increased biomass of bacteria, AMF, fungi, actinomycetes, and eukaryotes. This increase might result from increased root exudation at $P_{2.5}$, which we quantified using leaf (Pang et al. 2018). Together, these responses reveal that rhizosheath microbes were stimulated by $P_{2.5}$ and promoted co-growth of *L. chinensis* (Feng and Zhu 2019; DeForest et al. 2021; Luo et al. 2022). We will discuss the negative effects of rhizosheath microbes further in Sect. 4.3. Overall, these results support our hypothesis 2: P addition promoted belowground niche segregation by modifying the root morphology and rhizosheath microbial community composition of both species. The emergence of surplus niches at P_5 and $P_{12.5}$ can be attributed to these belowground niche differences.

Trade-offs in plant–microbe feedbacks

Trade-offs between plant internal P resorption and external soil P acquisition, influenced by plant–microbe feedbacks, greatly affect plant niche utilization (Fig. 10; Hata et al. 2018; Zhang et al. 2016). For both *C. aristatum* and *L. chinensis*, we observed significant trade-offs between the internal P abundance and external P acquisition along the P-addition gradient. This indicates that both species shaped their P-resorption and -acquisition strategies in response to P addition (Peng et al. 2023). However,

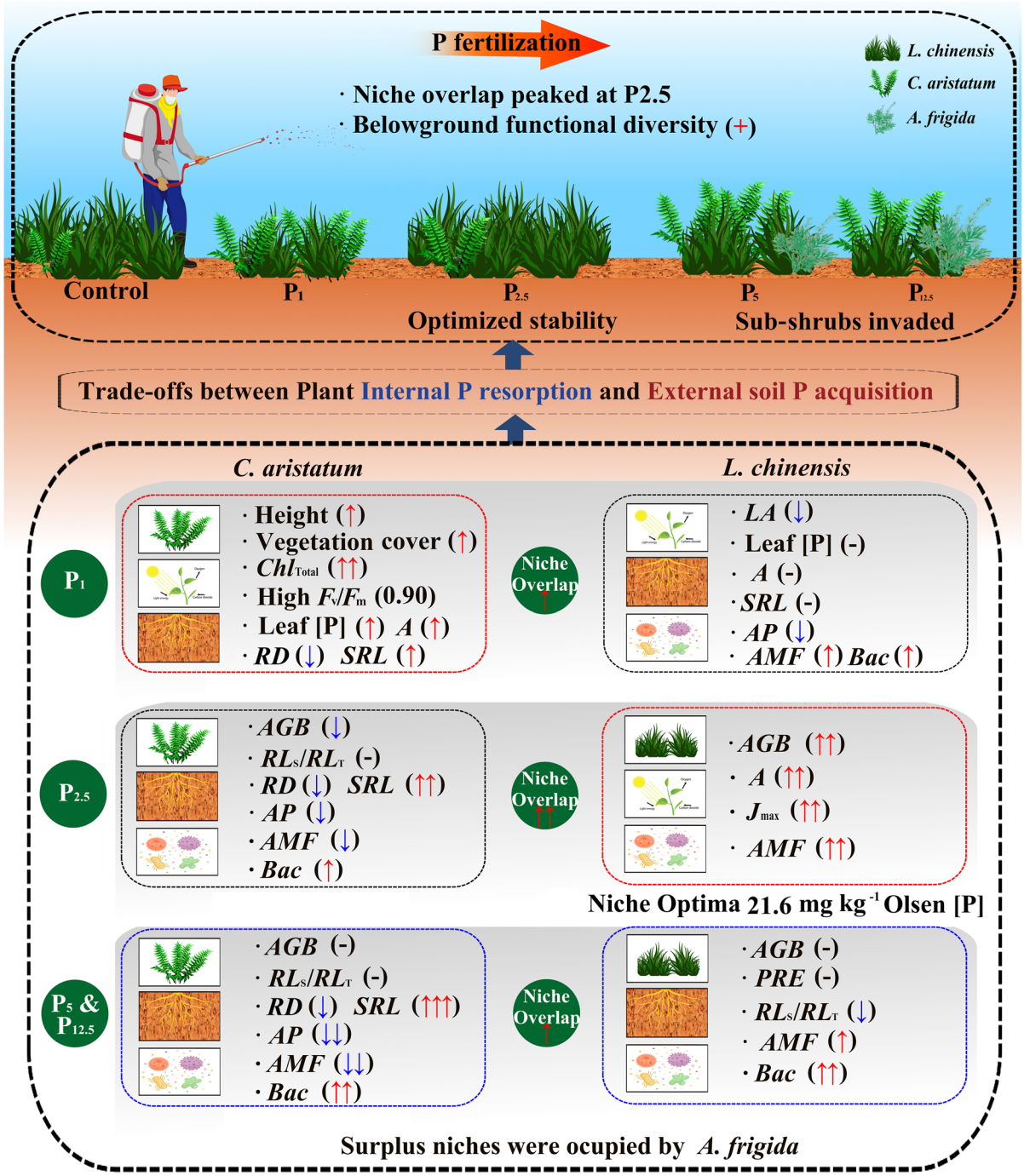

Fig. 10 A conceptual diagram of the effects of phosphorus (P) addition on niche characteristics and the above- and belowground differences between species and plant–microbe interactions under different P-addition levels. P_1, $P_{2.5}$, P_5, and $P_{12.5}$ represent P addition at 1, 2.5, 5, and 12.5 g P m^{-2} $year^{-1}$, respectively. Trait abbreviations as in Table S1. The symbols ↑, ↓, and - indicate increases, decreases, and maintained, respectively, in these traits

the response patterns of the two species differed greatly, and depended on their distinct plant–microbe interactions, resulting in different niche dynamics. For*C. aristatum*, the relative P abundance increased remarkably at $P_{12.5}$. This indicates that a severe N: P imbalance only occurred at $P_{12.5}$, and that N resorption by this species did not compensate for its N loss in leaves (Su et al. 2021). Interestingly, its rhizosheath microbial biomass N: P (*MBN: MBP*) remained relatively high, whereas leaf and rhizosheath microbial biomass C: N:P stoichiometry were mismatched. This indicates that *C. aristatum* did not efficiently obtain the limiting element (i.e. N) through its rhizosheath microbes; as a result, it failed to occupy an even larger niche at $P_{12.5}$. The cause for these phenomena is that *C. aristatum* and its rhizosheath microbial community are not closely related as in C_3plants (DeForest et al. 2021; Pathak and Nallapeta 2014). The similarity of the trends for total PLFAs of its rhizosheath and the bulk soil also suggests the lack of a powerful plant–microbe linkage for*C. aristatum* (Ven et al. 2019). Due to this functional mismatch, severe P enrichment in the rhizosheath of *C. aristatum* was observed at P_5 and $P_{12.5}$, and this was detrimental to the stability of the rhizosheath microbial community (He and Dijkstra 2015; Heuck et al. 2015; Spohn and Kuzyakov 2013).

Unlike for *C. aristatum*, the correlation between leaf and rhizosheath microbial C: P of *L. chinensis*was significant. This indicates a stronger plant–microbe linkage for P cycling (Moran 2017; Su et al. 2021; Wassen et al. 2021). The niche optima of this species presented at 21.6 mg kg^{-1} Olsen [P] ($P_{2.5}$ ~ P_5) might have resulted from this functional plant–microbe feedback (Wang et al. 2016). However, this linkage might become an obstacle for widening of the niches of*L. chinensis*when its companion microbes were suffering from a nutrient deficiency (Pathak and Nallapeta 2014). At P_5 and $P_{12.5}$, leaf N: P remained stable, but the rhizosheath *MBN*:*MBP* decreased significantly. The loss of relative dominance by this species at P_5 and $P_{12.5}$might be attributed to this imbalance between above- and belowground functions (Rejmánková and Sirová 2007; Su et al. 2021; Zhu et al. 2020). Moreover, presumably due to the plant–microbe imbalance at P_5 and $P_{12.5}$, *L. chinensis* did not occupy surplus niches, resulting in invasion by *A. frigida* (Babalola et al. 2020; Pathak and Nallapeta 2014; Tang et al. 2015). Overall, $P_{2.5}$ promoted both carbon assimilation and rhizosheath microbial biomass of *L. chinensis*, whereas P_5 and $P_{12.5}$ led to imbalanced N: P stoichiometry between *L. chinensis* and its rhizosheath microbes. These results support our hypothesis 3: a moderate level of P addition will promote a matched plant–microbe feedback of *L. chinensis*, but high P addition led to imbalanced N: P stoichiometry between plants and microbes.

Conclusion

Our results show that P fertilization changed the niche characteristics of the grassland ecosystem which was associated with changed above- and belowground plant morphology and physiology. *Leymus chinensis* presented the highest realized niche width along P-addition gradient, while P-addition exacerbated interspecific competition between *C. aristatum* and the dominant species (*L. chinensis*). The height similarity of *C. aristatum* and *L. chinensis* directly increased this competition, probably through increased competition for light. Low and high P-addition levels caused different degrees of competitive exclusion of *L. chinensis*, whereas a suitable and potentially optimal P-addition level ($P_{2.5}$) enhanced its biomass accumulation. The niche optima of *L. chinensis* presented at 21.6 mg kg^{-1} Olsen [P] ($P_{2.5}$ ~ P_5). At the same time, P fertilization drove differences in root architecture, morphology, and microbial mediation by *C. aristatum* and *L. chinensis* which was associated with mitigating their niche overlap, especially at P_5 and $P_{12.5}$. Furthermore, trade-offs between P resorption and acquisition were greatly altered by the distinct patterns of plant–microbe feedbacks along the P-addition gradient. Associated with functional mismatches in the plant–microbe systems of the two species, the niches of *C. aristatum* and *L. chinensis* did not widen at P_5 and $P_{12.5}$, and the surplus niches were occupied by an invasive sub-shrub (*A. frigida*). Taken together, our results highlight the importance of rhizosheath microbes in mediating trade-offs between above- and belowground co-responses of host plants along a P gradient, especially for the dominant species that strongly determined community productivity and stability. These insights could be applied to develop P-management guidelines for restoration of degraded grassland under future global climate change.

Author contributions Jirui Gong designed the experiment. Weiyuan Zhang, Siqi Zhang, and Xuede Dong performed sample preparation. Weiyuan Zhang performed the laboratory experiments, analyzed the data, drew figures and tables, and wrote the first draft. Jirui Gong and Hans Lambers made a major contribution to the final version. Siqi Zhang, Xuede Dong, Yuxia Hu, Guisen Yang, and Chenyi Yan contributed to the interpretation of the results and writing of the manuscript.

Funding This work was funded by the National Key R&D Program of China (Grant No. 2022YFF1303404) and National Natural Science Foundation of China (Grant No. 32230065). We are grateful to Inner Mongolia University for providing us with the study site and Laboratory analysis and Testing Center of State Key Laboratory of Earth Surface Processes and Resource Ecology for helping with the fieldwork and experiments.

Data availability The datasets generated during and/or analysed during the current study are available from the corresponding author on reasonable request.

Declarations

Competing interests The authors have no relevant financial or non-financial interests to disclose.

References

Aschehoug ET, Callaway RM (2014) Morphological variability in tree root architecture indirectly affects coexistence among competitors in the understory. Ecology 95:1731–1736. https://doi.org/10.1890/13-1749.1

Ashton IW, Miller AE, Bowman WD, Suding KN (2010) Niche complementarity due to plasticity in resource use: plant partitioning of chemical N forms. Ecology 91:3252–3260. https://doi.org/10.1890/09-1849.1

Austin MP, Meyers JA (1996) Current approaches to modelling the environmental niche of eucalypts: implication for management of forest biodiversity. For Ecol Manag 85:95–106. https://doi.org/10.1016/S0378-1127(96)03753-X

Ávila-Lovera E, Goldsmith GR, Kay KM, Funk JL (2021) Above- and below-ground functional trait coordination in the neotropical understory genus *Costus*. AoB Plants 14:plab073. https://doi.org/10.1093/aobpla/plab073

Babalola OO, Fadiji AE, Enagbonma BJ, Alori ET, Ayilara MS, Ayangbenro AS (2020) The nexus between plant and plant microbiome: revelation of the networking strategies. Front Microbiol 11:548037. https://doi.org/10.3389/fmicb.2020.548037/full

Bai Y, Wu J, Xing Q, Pan Q, Huang J, Yang D, Han X (2008) Primary production and rain use efficiency across a precipitation gradient on the Mongolia plateau. Ecology 89:2140–2153

Bai Y, Wu J, Clark CM, Naeem S, Pan Q, Huang J, Zhang L, Han X (2010) Tradeoffs and thresholds in the effects of nitrogen addition on biodiversity and ecosystem functioning: evidence from inner Mongolia grasslands. Global Change Biol 16:358–372. https://doi.org/10.1111/j.1365-2486.2009.01950.x

Baldarelli LM, Throop HL, Collins SL, Ward D (2021) Nutrient additions have direct and indirect effects on biocrust biomass in a long-term Chihuahuan Desert grassland experiment. J Arid Environ 184:104317. https://doi.org/10.1016/j.jaridenv.2020.104317

Barazetti AR, Simionato AS, Pérez-Navarro MO, dos Santos IMO, Modolon F, de Lima Andreata MF , Liuti G, Cely MVT, Chryssafidis AL, Dealis ML, Andrade G (2019) Formulations of arbuscular mycorrhizal fungi inoculum applied to soybean and corn plants under controlled and field conditions. Appl Soil Ecol 142:25–43. https://doi.org/10.1016/j.apsoil.2019.05.015

Boisson S, Monty A, Séleck M, Shutcha MN, Faucon M, Mahy G (2020) Ecological niche distribution along soil toxicity gradients: bridging theoretical expectations and metallophyte conservation. Ecol Mod 415:108861. https://doi.org/10.1016/j.ecolmodel.2019.108861

Bossio DA, Scow KM (1998) Impacts of carbon and flooding on soil microbial communities: phospholipid fatty acid profiles and substrate utilization patterns. Microb Ecol 35:265–278. https://doi.org/10.1007/s002489900082

Brookes PC, Powlson DS, Jenkinson DS (1982) Measurement of microbial biomass phosphorus in soil. Soil Biol Biochem 14:319–329. https://doi.org/10.1016/0038-0717(82)90001-3

Burns RG, DeForest JL, Marxsen J, Sinsabaugh RL, Stromberger ME, Wallenstein MD, Weintraub MN, Zoppini A (2013) Soil enzymes in a changing environment: current knowledge and future directions. Soil Biol Biochem 58:216–234. https://doi.org/10.1016/j.soilbio.2012.11.009

Chen J, Wang Q, Li M, Liu F, Li W (2016) Does the different photosynthetic pathway of plants affect soil respiration in a subtropical wetland? Ecol Evol 6:8010–8017. https://doi.org/10.1002/ece3.2523

Cleveland CC, Houlton BZ, Smith WK, Marklein AR, Reed SC, Parton W, Del Grosso SJ, Running SW (2013) Patterns of new versus recycled primary production in the terrestrial biosphere. P Natl Acad Sci USA 110:12733–12737

Cohen D (1994) Modelling the coexistence of annual and perennial plants in temporally varying environments. Plant Spec Biol 9:1–10

Copeland SM, Munson SM, Bradford JB, Butterfield BJ, Gunnell KL (2019) Long-term plant community trajectories suggest divergent responses of native and non-native perennials and annuals to vegetation removal and seeding treatments. Restor Ecol 27:821–831. https://doi.org/10.1111/rec.12928

Cordell D, Drangert J, White S (2009) The story of phosphorus: global food security and food for thought. Global Environ Change 19:292–305. https://doi.org/10.1016/j.gloenvcha.2008.10.009

DeForest JL (2019) Chronic phosphorus enrichment and elevated pH suppresses *Quercus* spp. leaf litter decomposition in a temperate forest. Soil Biol Biochem 135:206–212. https://doi.org/10.1016/j.soilbio.2019.05.005

DeForest JL, Dorkoski R, Freedman ZB, Smemo KA (2021) Multi-year soil microbial and extracellular phosphorus enzyme response to lime and phosphate addition in temperate hardwood forests. Plant Soil 464:391–404. https://doi.org/10.1007/s11104-021-04947-4

Demmig-Adams B, Adams WW III, Barker DH, Logan BA, Bowling DR, Verhoeven AS (1996) Using chlorophyll fluorescence to assess the fraction of absorbed light allocated to thermal dissipation of excess excitation. Physiol Plant 98:253–264. https://doi.org/10.1034/j.1399-3054.1996.980206.x

Díaz S, Lavorel S, McIntyre S, Falczyk V, Casanoves F, Milchunas DG, Skarpe C, Rusch G, Sternberg M, Noy-Meir I, Landsberg J, Zhang W, Clark H, Campbell BD (2006) Plant trait responses to grazing – a global synthesis. Global Change Biol 13:313–341. https://doi.org/10.1111/j.1442-1984.1994.tb00075.x

Du E, Terrer C, Pellegrini AFA, Ahlström A, van Lissa CJ, Zhao X, Xia N, Wu X, Jackson RB (2020) Global patterns of terrestrial nitrogen and phosphorus limitation. Nat Geosci 13:221–226. https://doi.org/10.1038/s41561-019-0530-4

Fargašová A (1996) Inhibitive effect of organotin compounds on the chlorophyll content of the green freshwater alga *Scenedesmus quadricauda*. Bull Environ Contam Toxicol 57:99–106. https://doi.org/10.1007/s001289900161

Farquhar GD, von Caemmerer S, Berry JA (1980) A biochemical model of photosynthetic CO_2 assimilation in leaves of C_3 species. Planta 149:78–90. https://doi.org/10.1007/bf00386231

Feng J, Zhu B (2019) A global meta-analysis of soil respiration and its components in response to phosphorus addition. Soil Biol Biochem 135:38–47. https://doi.org/10.1016/j.soilbio.2019.04.008

Fiorentini M, Zenobi S, Giorgini E, Basili D, Conti C, Pro C, Monaci E, Orsini R (2019) Nitrogen and chlorophyll status determination in durum wheat as influenced by fertilization and soil management: preliminary results. PLoS ONE 14:e0225126. https://doi.org/10.1371/journal.pone.0225126

Fornara DA, Tilman D (2009) Ecological mechanisms associated with the positive diversity—productivity relationship in an N-limited grassland. Ecology 90:408–418. https://doi.org/10.1890/08-0325.1

Freschet GT, Roumet C, Comas LH, Weemstra M, Bengough AG, Rewald B, Bardgett RD, De Deyn GB, Johnson D, Klimešová J (2020) Root traits as drivers of plant and ecosystem functioning: current understanding, pitfalls and future research needs. New Phytol 232:1123–1158. https://doi.org/10.1111/nph.17072

García-Palacios P, Gross N, Gaitán J, Maestre FT (2018) Climate mediates the biodiversity–ecosystem stability relationship globally. Proc Natl Acad Sci USA 115:8400–8405. https://doi.org/10.1073/pnas.1800425115

Garlick K, Drew RE, Rajaniemi TK (2021) Root responses to neighbors depend on neighbor identity and resource distribution. Plant Soil 467:227–237. https://doi.org/10.1007/s11104-021-05083-9

Ghannoum O, Conroy JP (2007) Phosphorus deficiency inhibits growth in parallel with photosynthesis in a C3 (Panicum laxum) but not two C4 (P. coloratum and Cenchrus ciliaris) grasses. Funct Plant Biol 34:72–81. https://doi.org/10.1071/FP06253

Ghannoum O, Paul MJ, Ward JL, Beale MH, Corol DI, Conroy JP (2008) The sensitivity of photosynthesis to phosphorus deficiency differs between C_3 and C_4 tropical grasses. Funct Plant Biol 35:213–221. https://doi.org/10.1071/fp07256

Gong S, Zhang T, Guo J (2020) Warming and nitrogen deposition accelerate soil phosphorus cycling in a temperate meadow ecosystem. Soil Res 58:109–115. https://doi.org/10.1071/sr19114

Graux AI, Resmond R, Casellas E, Delaby L, Faverdin P, Le Bas C, Ripoche D, Ruget F, Thérond O, Vertès F, Peyraud JL (2020) High-resolution assessment of French grassland dry matter and nitrogen yields. Eur J Agron 112:125952. https://doi.org/10.1016/j.eja.2019.125952

Guerrieri R, Belmecheri S, Ollinger SV, Asbjornsen H, Jennings K, Xiao J, Stocker BD, Martin M, Hollinger DY, Bracho-Garrillo R, Clark K, Dore S, Kolb T, Munger JW, Novick K, Richardson AD (2019) Disentangling the role of photosynthesis and stomatal conductance on rising forest water-use efficiency. Proc Natl Acad Sci 16:16909–16914. https://doi.org/10.1073/pnas.1905912116

Güsewell S (2004) N:P ratios in terrestrial plants: variation and functional significance. New Phytol 164:243–266. https://doi.org/10.2307/1514768

Happonen K, Virkkala AM, Kemppinen J, Niittynen P, Luoto M (2022) Relationships between aboveground plant traits and carbon cycling in tundra plant communities. J Ecol 110:700–716. https://doi.org/10.1111/1365-2745.13832

Harpole WS, Suding KN (2011) A test of the niche dimension hypothesis in an arid annual grassland. Oecologia 166:197–205. https://doi.org/10.2307/41499822

Hata K, Osawa T, Hiradate S, Kachi N (2018) Soil erosion alters soil chemical properties and limits grassland plant establishment on an oceanic island even after goat eradication. Restor Ecol 27:333–342. https://doi.org/10.1111/rec.12854

Hayes P, Turner BL, Lambers H, Laliberté E (2014) Foliar nutrient concentrations and resorption efficiency in plants of contrasting nutrient-acquisition strategies along a 2-million-year dune chronosequence. J Ecol 102:396–410. https://doi.org/10.1111/1365-2745.12196

He M, Dijkstra FA (2015) Phosphorus addition enhances loss of nitrogen in a phosphorus-poor soil. Soil Biol Biochem 82:99–106. https://doi.org/10.1016/j.soilbio.2014.12.015

Heuck C, Weig A, Spohn M (2015) Soil microbial biomass C:N:P stoichiometry and microbial use of organic phosphorus. Soil Biol Biochem 85:119–129. https://doi.org/10.1016/j.soilbio.2015.02.029

Higgins SI, O'Hara RB, Römermann C (2012) A niche for biology in species distribution models. J Biogeogr 39:2091–2095. https://doi.org/10.1111/jbi.12029

Holt RD (2009) Bringing the Hutchinsonian niche into the 21st century: ecological and evolutionary perspectives. Proc Natl Acad Sci USA 106:19659–19665. https://doi.org/10.2307/25593251

Huang ZQ, Ran SS, Fu YR, Wan XH, Song X, Chen YX, Yu ZP (2022) Functionally dissimilar neighbors increase tree water use efficiency through enhancement of leaf

phosphorus concentration. J Appl Ecol 58:2833–2842. https://doi.org/10.1111/1365-2745.13941

Jacoby RP, Kopriva S (2019) Metabolic niches in the rhizosphere microbiome: new tools and approaches to analyse metabolic mechanisms of plant–microbe nutrient exchange. J Exp Bot 70:1087–1094. https://doi.org/10.1093/jxb/ery438

Kidd DR, Ryan MH, Hahne D, Haling RE, Lambers H, Sandral GA, Simpson R, Cawthray G (2018) The carboxylate composition of rhizosheath and root exudates from twelve species of grassland and crop legumes with special reference to the occurrence of citramalate. Plant Soil 424:389–403. https://doi.org/10.1007/s11104-017-3534-0

Kramer-Walter KR, Bellingham PJ, Millar TR, Smissen RD, Richardson SJ, Laughlin DC (2016) Root traits are multidimensional: specific root length is independent from root tissue density and the plant economic spectrum. J Ecol 104:1299–1310. https://doi.org/10.1111/1365-2745.12562

Krüger GHJ, Jordaan A, Tiedt LR, Strasser RJ, Kilbourn Louw M, Berner JM (2017) Opportunistic survival strategy of *Welwitschia mirabilis*: recent anatomical and ecophysiological studies elucidating stomatal behaviour and photosynthetic potential. Botany 95:1109–1123. https://doi.org/10.1139/cjb-2017-0095

Lejeune KD, Suding KN, Seastedt TR (2006) Nutrient availability does not explain invasion and dominance of a mixed grass prairie by the exotic forb *Centaurea diffusa* Lam. Appl Soil Ecol 32:98–110. https://doi.org/10.1016/j.apsoil.2005.01.009

Levey M, Timm S, Mettler-Altmann T, Borghi GL, Koczor M, Arrivault S, Weber APM, Bauwe H, Gowik U, Westhoff P (2018) Efficient 2-phosphoglycolate degradation is required to maintain carbon assimilation and allocation in the C_4 plant *Flaveria bidentis* J Exp Bot 70:575–587. https://doi.org/10.1093/jxb/ery370

Li L, Li SM, Sun JH, Zhou LL, Bao XG, Zhang HG, Zhang FS (2007) Diversity enhances agricultural productivity via rhizosphere phosphorus facilitation on phosphorus-deficient soils. Proc Natl Acad Sci USA 104:11192–11196. https://doi.org/10.1073/pnas.0704591104

Li SX, Wang ZH, Malhi SS, Li SQ, Gao YJ, Tian XH (2009) Nutrient and water management effects on crop production, and nutrient and water use efficiency in dryland areas of China. Adv Agro 102:223–265. https://doi.org/10.1016/S0065-2113(09)01007-4

Li LJ, Zeng DH, Mao R, Yu ZY (2012) Nitrogen and phosphorus resorption of Artemisia scoparia, Chenopodium acuminatum, Cannabis sativa, and Phragmites communis under nitrogen and phosphorus additions in a semiarid grassland, China. Plant Soil Environ 58:446–451. https://doi.org/10.17221/6339-PSE

Li L, Yang H, Peng L, Ren W, Gong J, Liu P, Wu X, Huang F (2019) Comparative study reveals insights of sheepgrass (*Leymus Chinensis*) coping with phosphate-deprived stress condition. Front Plant Sci 10:170. https://doi.org/10.3389/fpls.2019.00170

Li Z, Liang M, Li Z, Mariotte P, Tong X, Zhang J, Dong L, Zheng Y, Ma W, Zhao L, Wang L, Wen L, Tuvshintogtokh I, Gornish ES, Dang Z, Liang C, Li FY (2021) Plant functional groups mediate effects of climate and soil factors on species richness and community biomass in grasslands of Mongolian Plateau. J Plant Ecol 14:679–691. https://doi.org/10.1093/jpe/rtab021

Lie Z, Zhou G, Huang W, Kadowaki K, Tissue DT, Yan J, Peñuelas J, Sardans J, Li Y, Liu S, Chu G, Meng Z, He X, Liu J (2022) Warming drives sustained plant phosphorus demand in a humid tropical forest. Global Change Biol 28:4085–4096. https://doi.org/10.1111/gcb.16194

Liu M, Zhang Z, He Q, Wang H, Li X, Schoer J (2014) Exogenous phosphorus inputs alter complexity of soil-dissolved organic carbon in agricultural riparian wetlands. Chemosphere 95:572–580. https://doi.org/10.1016/j.chemosphere.2013.09.117

Liu C, Liu Y, Guo K, Qiao X, Zhao H, Wang S, Zhang L, Cai X (2018) Effects of nitrogen, phosphorus and potassium addition on the productivity of a karst grassland: plant functional group and community perspectives. Ecol Eng 117:84–95. https://doi.org/10.1016/j.ecoleng.2018.04.008

Luo Q, Gong J, Yang L, Li X, Pan Y, Liu M, Zhai Z, Baoyin T (2017) Impacts of nitrogen addition on the carbon balance in a temperate semiarid grassland ecosystem. Biol Fert Soils 53:911–927. https://doi.org/10.1007/s00374-017-1233-x

Luo R, Kuzyakov Y, Zhu B, Qiang W, Zhang Y, Pang X (2022) Phosphorus addition decreases plant lignin but increases microbial necromass contribution to soil organic carbon in a subalpine forest. Global Change Biol 13:28. https://doi.org/10.1111/gcb.16205

Lynch J, Brown K (2008) Root strategies for phosphorus acquisition. In: White P, Hammond J (eds) The ecophysiology of plant-phosphorus interaction, vol 7. Springer, Berlin, pp 83–116. https://doi.org/10.1007/978-1-4020-8435-5_5

Lynch JP, Ho MD (2005) Rhizoeconomics: carbon costs of phosphorus acquisition. Plant Soil 269:45–56. https://doi.org/10.1007/s11104-004-1096-4

Ma Z, Guo D, Xu X, Lu M, Bardgett R, Eissenstat DM, McCormack ML, Hedin LO (2018) Evolutionary history resolves global organization of root functional traits. Nature 555:94–97. https://doi.org/10.1038/nature26163

Martini D, Pacheco-Labrador J, Perez-Priego O, Migliavacca M (2019) Nitrogen and phosphorus effect on sun-induced fluorescence and gross primary productivity in Mediterranean grassland. Remote Sens-Basel 11:2562. https://doi.org/10.3390/rs11212562

Maxwell K, Johnson GN (2000) Chlorophyll fluorescence—a practical guide. J Exp Bot 51:659–668. https://doi.org/10.1093/jexbot/51.345.659

Mo Q, Li ZA, Sayer EJ, Lambers H, Li Y, Zou B, Tang J, Heskel M, Ding Y, Wang F, Ostertag R (2019) Foliar phosphorus fractions reveal how tropical plants maintain photosynthetic rates despite low soil phosphorus availability. Funct Ecol 33:503–513. https://doi.org/10.1111/1365-2435.13252

Moran R, Wong I, Rodríguez F, Somonte D, de la Torre D, Dominguez L, Valdivia AN, Alvarez I, González N, Paneque Y, Heredia CEP, Mora N, Sánchez I, Rodríguez RF, Galdós L, Verdecia-Mogena A (2017) From the rhizosphere to a bioproduct. The role of plant–microbe interactions. In: 11th International Congress on Plant

Biotechnology and Agriculture BIOVEG. https://www.researchgate.net/publication/318147336_From_the_rhizosphere_to_a_bioproduct_The_role_of_plant-microbe_interactions. Accessed May 2017

Onoda Y, Hikosaka K, Hirose T (2004) Allocation of nitrogen to cell walls decreases photosynthetic nitrogen-use efficiency. Funct Ecol 18:419–425. https://doi.org/10.2307/3599203

Pang J, Bansal R, Zhao H, Bohuon E, Lambers H, Ryan MH, Ranathunge K, Siddique KMH (2018) The carboxylate-releasing phosphorus-mobilising strategy could be proxied by foliar manganese concentration in a large set of chickpea germplasm under low phosphorus supply. New Phytol 219:518–529. https://doi.org/10.1111/nph.15200

Pathak KV, Nallapeta S (2014) Plant–microbial interaction: a dialogue between two dynamic bioentities. In: Kavi KPB, Rajib B, Prashanth S (eds) Agricultural bioinformatics. Springer, Berlin, pp 259–272. https://doi.org/10.1007/978-81-322-1880-7_15

Peng ZY, Wu YT, Guo LL, Yang L, Wang B, Wang X, Liu WX, Su YJ, Wu J, Liu LL (2023) Foliar nutrient resorption stoichiometry and microbial phosphatase catalytic efficiency together alleviate the relative phosphorus limitation in forest ecosystems. New Phytol 238:1033–1044. https://doi.org/10.1111/nph.18797

Phoenix GK, Johnson DA, Muddimer SP, Leake JR, Cameron DD (2020) Niche differentiation and plasticity in soil phosphorus acquisition among co-occurring plants. Nat Plants 6:349–354. https://doi.org/10.1038/s41477-020-0624-4

Pianka ER (1973) The structure of lizard communities. Annu Rev Ecol Evol Syst 4:53–74. https://doi.org/10.1146/annurev.es.04.110173.000413

Qaswar M, Li D, Huang J, Han T, Ahmed W, Abbas M, Zhang L, Du J, Khan ZH, Ullah S, Zhang H, Wang B (2020) Interaction of liming and long-term fertilization increased crop yield and phosphorus use efficiency (*PUE*) through mediating exchangeable cations in acidic soil under wheat–maize cropping system. Sci Rep-UK 10:19828. https://doi.org/10.1038/s41598-020-76892-8

Raiesi F, Beheshti A (2014) Soil specific enzyme activity shows more clearly soil responses to paddy rice cultivation than absolute enzyme activity in primary forests of northwest Iran. Appl Soil Ecol 75:63–70. https://doi.org/10.1016/j.apsoil.2013.10.012

Reed SC, Townsend AR, Davidson EA, Cleveland CC (2012) Stoichiometric patterns in foliar nutrient resorption across multiple scales. New Phytol 196:173–180. https://doi.org/10.1111/j.1469-8137.2012.04249.x

Reich PB, Wright IJ, Cavender-Bares JC, Craine M, Oleksyn J, Walters MB (2003) The evolution of plant functional variation: traits, spectra, and strategies. Int J Plant Sci 164:S143–S164. https://doi.org/10.1086/374368

Rejmánková E, Sirová D (2007) Wetland macrophyte decomposition under different nutrient conditions: relationships between decomposition rate, enzyme activities and microbial biomass. Soil Biol Biochem 39:526–538. https://doi.org/10.1016/j.soilbio.2006.08.022

Ren F, Song W, Chen L, Mi Z, Zhang Z, Zhu W, Zhou H, Cao G, He JS (2016) Phosphorus does not alleviate the negative effect of nitrogen enrichment on legume performance in an alpine grassland. J Plant Ecol 10:822–830. https://doi.org/10.1093/jpe/rtw089

Richardson AE, Lynch JP, Ryan PR, Delhaize E, Smith FA, Smith SE, Harvey PR, Ryan MH, Veneklaas EJ, Lambers H, Oberson A, Culvenor RA, Simpson RJ (2011) Plant and microbial strategies to improve the phosphorus efficiency of agriculture. Plant Soil 349:121–156

Sanaei A, Ali A (2019) What is the role of perennial plants in semi-steppe rangelands? Direct and indirect effects of perennial on annual plant species. Ecol Indic 98:389–396. https://doi.org/10.1016/j.ecolind.2018.11.012

Shi B, Ling X, Cui H, Song W, Gao Y, Sun W (2020) Response of nutrient resorption of Leymus chinensis to nitrogen and phosphorus addition in a meadow steppe of northeast China. Plant Biol 22:1123–1132. https://doi.org/10.1111/plb.13153

Shi J, Gong J, Baoyin T, Luo Q, Zhai Z, Zhu C, Yang B, Wang B, Zhang Z, Li X (2021) Short-term phosphorus addition increases soil respiration by promoting gross ecosystem production and litter decomposition in a typical temperate grassland in northern China. Catena 197:104952. https://doi.org/10.1016/j.catena.2020.104952

Shi JY, Gong JR, Li XB, Zhang ZH, Zhang WY, Li Y, Song LY, Zhang SQ, Dong JJ, Baoyin TT (2023) Phosphorus application promotedthe sequestration of orthophosphate within soil microorganisms and regulatedthe soil solution P supply in a temperate grassland in northern China: a ^{31}P NMR study. Soil Tillage Res 227:105612. https://doi.org/10.1016/j.still.2022.105612

Shipley B (2006) Net assimilation rate, specific leaf area and leaf mass ratio: which is most closely correlated with relative growth rate? A meta-analysis. Funct Ecol 20:565–574. https://doi.org/10.1111/j.1365-2435.2006.01135.x

Silvertown J (2004) Plant coexistence and the niche. Trends Ecol Evol 19:605–611. https://doi.org/10.1016/j.tree.2004.09.003

Simpson EH (1949) Measurement of diversity. Nature 163:688

Slot M, Winter K (2017) *In situ* temperature relationships of biochemical and stomatal controls of photosynthesis in four lowland tropical tree species. Plant Cell Environ 40:3055–3068. https://doi.org/10.1111/pce.13071

Smith S (2011) Roles of arbuscular mycorrhizas in plant nutrition and growth: new paradigms from cellular to ecosystem scales. Annu Rev Plant Biol 62:227–250. https://doi.org/10.1146/annurev-arplant-042110-103846

Smith B (2022) Declining global leaf nitrogen content: smart resource use by flexible plants? New Phytol 235:1683–1685. https://doi.org/10.1111/nph.18354

Spohn M, Kuzyakov Y (2013) Phosphorus mineralization can be driven by microbial need for carbon. Soil Biol Biochem 61:69–75. https://doi.org/10.1016/j.soilbio.2013.02.013

Spohn M, Ermak A, Kuzyakov Y (2013) Microbial gross organic phosphorus mineralization can be stimulated by root exudates–a P isotopic dilution study. Soil Biol Biochem 65:254–263. https://doi.org/10.1016/j.soilbio.2013.05.028

Strickland MS, Rousk J (2010) Considering fungal:bacterial dominance in soils – methods, controls, and ecosystem

implications. Soil Biol Biochem 42:1385–1395. https://doi.org/10.1016/j.soilbio.2010.05.007

Su Y, Ma X, Le J, Li K, Han W, Liu X (2021) Decoupling of nitrogen and phosphorus in dominant grass species in response to long-term nitrogen addition in an alpine grassland in Central Asia. Plant Ecol 222:1–14. https://doi.org/10.1007/s11258-020-01103-3

Sullivan BW, Alvarez-Clare S, Castle SC, Porder S, Reed SC, Schreeg L, Townsend AR, Cleveland CC (2014) Assessing nutrient limitation in complex forested ecosystems: alternatives to large-scale fertilization experiments. Ecology 95:668–681. https://doi.org/10.1890/13-0825.1

Sun Q, Yamada T, Han Y, Takano T (2021) Influence of salt stress on C_4 photosynthesis in *Miscanthus sinensis* Anderss. Plant Biol 23:44–56. https://doi.org/10.1111/plb.13192

Tang ZS, An H, Shangguan ZP (2015) The impact of desertification on carbon and nitrogen storage in the desert steppe ecosystem. Ecol Eng 84:92–99. https://doi.org/10.1016/j.ecoleng.2015.07.023

Tran CTK, Watts-Williams SJ, Smernik RJ, Cavagnaro TR (2020) Effects of plant roots and arbuscular mycorrhizas on soil phosphorus leaching. Sci Total Environ 722:137384. https://doi.org/10.1016/j.scitotenv.2020.137847

Turner BL, Brenes-Arguedas T, Condit R (2018) Pervasive phosphorus limitation of tree species but not communities in tropical forests. Nature 555:367–370. https://doi.org/10.1038/nature25789

van der Sande MT, Arets EJMM, Peña-Claros M, Hoosbeek MR, Cáceres-Siani Y, van der Hout P, Poorter L (2017) Soil fertility and species traits, but not diversity, drive productivity and biomass stocks in a Guyanese tropical rainforest. Funct Ecol 32(2):461–474. https://doi.org/10.1111/1365-2435.12968

Vance ED (1987) An extracted method for measuring soil microbial biomass C. Soil Biol Biochem 19:703–707. https://doi.org/10.1016/0038-0717(87)90052-6

Ven A, Verlinden MS, Verbrugge NE, Vicca S (2019) Experimental evidence that phosphorus fertilization and arbuscular mycorrhizal symbiosis can reduce the carbon cost of phosphorus uptake. Funct Ecol 33:1–11. https://doi.org/10.1111/1365-2435.13452

Walk TC, Jaramillo R, Lynch JP (2006) Architectural tradeoffs between adventitious and basal roots for phosphorus acquisition. Plant Soil 279:347–366. https://doi.org/10.2307/24125291

Wang J, Wu Y, Zhou J, Bing H, Sun H (2016) Carbon demand drives microbial mineralization of organic phosphorus during the early stage of soil development. Biol Fert Soils 52:825–839. https://doi.org/10.1007/s00374-016-1123-7

Wang JH, Cai YF, Li SF, Zhang SB (2020) Photosynthetic acclimation of rhododendrons to light intensity in relation to leaf water-related traits. Plant Ecol 221:407–420. https://doi.org/10.1007/s11258-020-01019-y

Warren CR, Adams MA, Chen ZL (2000) Is photosynthesis related to concentrations of nitrogen and rubisco in leaves of Australian native plants? Funct Plant Biol 27:407–416. https://doi.org/10.1071/PP98162

Wassen MJ, Schrader J, van Dijk J, Eppinga MB (2021) Phosphorus fertilization is eradicating the niche of northern Eurasia' s threatened plant species. Nat Ecol Evol 5:1–7. https://doi.org/10.1038/s41559-020-01323-w

Wen Z, Li H, Shen Q, Tang X, Xiong C, Li H, Pang J, Ryan MH, Lambers H, Shen J (2019) Trade-offs among root morphology, exudation and mycorrhizal symbioses for phosphorus-acquisition strategies of 16 crop species. New Phytol 223:882–895. https://doi.org/10.1111/nph.15833

Wen Z, White PJ, Shen J, Lambers H (2021) Linking root exudation to belowground economic traits for resource acquisition. New Phytol 233:1620–1635. https://doi.org/10.1111/nph.17854

Wijesinghe DK, John EA, Hutchings MJ (2005) Does pattern of soil resource heterogeneity determine plant community structure? An experimental investigation. J Ecol 93:99–112. https://doi.org/10.1111/j.0022-0477.2004.00934.x

Wright IJ, Reich PB, Cornelissen JHC, Falster DS, Garnier E, Hikosaka K, Lamont BB, Lee W, Oleksyn J, Osada N, Poorter H, Villar R, Warton DI, Westoby M (2005) Assessing the generality of global leaf trait relationships. New Phytol 166:485–496. https://doi.org/10.1111/j.1469-8137.2005.01349.x

Xiao L, Liu G, Li P, Li Q, Xue S (2020) Ecoenzymatic stoichiometry and microbial nutrient limitation during secondary succession of natural grassland on the Loess Plateau, China. Soil Tillage Res 200:104605. https://doi.org/10.1016/j.still.2020.104605

Xu B, Yang XC, Tao WG, Miao JM, Yang Z, Liu HQ, Jin YX, Zhu XH, Qin ZH, Lv HY, Li JY (2013) MODIS-based remote-sensing monitoring of the spatiotemporal patterns of China's grassland vegetation growth. Int J Remote Sens 34:3867–3878. https://doi.org/10.1080/01431161.2012.762696

Yan N, Wang XQ, Xu XF, Guo DP, Wang ZD, Zhang JZ, Hyde KD, Liu HL (2013) Plant growth and photosynthetic performance of *Zizania latifolia* are altered by endophytic *Ustilago esculenta* infection. Physiol Mol Plant Pathol 83:75–83. https://doi.org/10.1016/j.pmpp.2013.05.005

Yang H (2018) Effects of nitrogen and phosphorus addition on leaf nutrient characteristics in a subtropical forest. Trees 32:383–391. https://doi.org/10.1007/s00468-017-1636-1

Ye ZP (2007) A new model for relationship between irradiance and the rate of photosynthesis in *Oryza sativa* Photosynthetica 45:637–640. https://doi.org/10.1007/s11099-007-0110-5

Yin X, Struik PC (2011) C_3 and C_4 photosynthesis models: an overview from the perspective of crop modelling. NJAS-Wagen J Life Sci 57:27–38. https://doi.org/10.1016/j.njas.2009.07.001

Yu RP, Li XX, Xiao ZH, Lambers H, Li L (2020) Phosphorus facilitation and covariation of root traits in steppe species. New Phytol 226:1285–1298. https://doi.org/10.1111/nph.16499

Zhang D, Zhang C, Tang X, Li H, Zhang F, Rengel Z, Whalley WR, Davies WJ, Shen J (2016) Increased soil phosphorus availability induced by faba bean root exudation stimulates root growth and phosphorus uptake in

neighbouring maize. New Phytol 209:823–831. https://doi.org/10.1111/nph.13613

Zhou R, Yu X, Kjær KH, Rosenqvist E, Ottosen CO, Wu Z (2015) Screening and validation of tomato genotypes under heat stress using F_v/F_m to reveal the physiological mechanism of heat tolerance. Environ Exp Bot 118:1–11. https://doi.org/10.1016/j.envexpbot.2015.05.006

Zhou T, Wang L, Sun X, Wang X, Chen Y, Rengel Z, Liu W, Yang W (2019) Light intensity influence maize adaptation to low P stress by altering root morphology. Plant Soil 447:183–197. https://doi.org/10.1007/s11104-019-04259-8

Zhou M, Guo Y, Sheng J, Yuan Y, Zhang WH, Bai W (2022) Using anatomical traits to understand root functions across root orders of herbaceous species in a temperate steppe. New Phytol 234:422–434. https://doi.org/10.1111/nph.17978

Zhu X, Liu M, Kou Y, Liu D, Liu Q, Zhang Z, Jiang Z, Yin H (2020) Differential effects of N addition on the stoichiometry of microbes and extracellular enzymes in the rhizosphere and bulk soils of an alpine shrubland. Plant Soil 449:285–301. https://doi.org/10.1007/s11104-020-04468-6